Investigating the relevance of simulated urination for a urethra-on-a-chip

Leila Hollis, MSc Candidate, Universiteit Utrecht
Intern, Department of Experimental Urology, Regenerative Medicine Center Utrecht
16 November 2022

porcine urethral epithelial cells

I would like to acknowledge those that helped this project bloom.

My most heartful gratitude to:

Dr. Petra de Graaf, for teaching me, guiding me, supporting me, allowing me to cry, and being my mom-away-from-mom.

Eline Kuijt, for countless hours spent helping with experiments, making sections, proofreading, giving advice, hosting writing days, answering numerous questions, and making the lab radiant and fun.

Roos van Dam, for her many valuable insights and contributions in the areas of immunostaining, qPCR, and more.

George Tsachouridis of UMCU, for his expertise and perspective.

Everyone at the RMCU, particularly the Nephrology group, for lending supplies, offering suggestions, and being a source of knowledge and experience.

Flora Vivensang, for her commiseration and for the long days and late nights spent working together, without which this report might never have been finished.

My family, Camron, Minoo, and Marcus Hollis, for being on-call 24/7 to support me by any and every means necessary from 7,500 kilometers away.

1 Abstract

Introduction Urethral stricture disease (USD) is prevalent among older men and can necessitate urethroplasty and tissue grafting. Regenerative medicine has the potential to create new therapies for USD using advanced organ-on-a-chip (OOC) models. Parameters must be optimized in OOC to create in-vivo-accurate models, and this study investigates the role of flow intermittent in culturing urethral cells with physiological phenotypes.

Methods Porcine urethral epithelial cells (pUECs) and human buccal mucosa cells (hBMCs) were cultured, and one medium was optimized to support them both. The cells underwent flow experiments in which they were subject to constant, intermittent, or no shear stress. Some of these cells were fluorescently stained for zonula occludins-1 (ZO-1), as well as other markers, and imaged, while the others were processed for use in quantitative polymerase chain reaction (qPCR) assays. SEM images made from pig penile tissue were analyzed along with fluorescent cell images for alignment to flow and elongation. Statistical analysis was performed for comparison between different shear stress conditions.

Results Intermittent flow led to significantly more elongated pUECs than those under constant flow or in tissue and significantly less aligned cells than in tissue. hBMCs were not quantified.

Conclusions Intermittent flow alone does not induce physiological morphology in pUECs. Functional metrics are needed before drawing further conclusions. Comparison to hBMCs should be done, and other parameters for recapitulating the native urethra should be considered for future iterations of the in-vitro urethra model.

Graphical Abstract

2 Layman's Summary

Researchers around the globe are out there right now creating tiny organs in channels less than a millimeter wide! Not only is this as fun as it sounds, but it also serves an important purpose. In the field of regenerative medicine, we work on ways to regenerate tissue that has been injured so that it can get back to the way it once was, or at least as close as possible. One strategy for this kind of investigation is to make a small model of the organ of interest, so that we can develop techniques without using an animal as a test subject. In urology, this is a particularly attractive route since human penile anatomy is quite unique, even compared to close relatives, so animal models don't adequately represent how a therapy might work in the clinic. An organ-on-a-chip, as it's called, ideally has all the important characteristics that can support cells from the organ of interest and keep them looking and behaving like they do in the body. Some important aspects could be the material of the chip, the combination of cells used, and the conditions the cells are exposed to.

One of the most common urogenital diseases among older men is urethral stricture disease (USD), in which scar tissue partially blocking the urethra causes issues with urination, ejaculation, and urinary tract infections. In most cases it's caused by catheterization, which involves inserting a tube into the bladder through the urethra in order to drain one's urine and is indicated in a number of scenarios, being performed as many as 200 times per minute across the globe. For cases of USD in which the scarred area is relatively large, greater than 2cm, surgery is needed to cut this area of the urethra out and replace it with new epithelium, or skin, as a graft. The number one choice for this graft among urologists is buccal mucosa, the epithelium that lines the inside of our cheeks, since it's easy to reach and performs a similar job as the urethral epithelium, that is, acting as a barrier between the outside world and our inner tissues. However, when tissue is taken from another part of your body, it leaves behind a wound, which can lead to pain and complications of its own. In addition, the substituted tissue doesn't perfectly match up with the organ that it's moved to.

Ultimately, our lab would like to create a urethra-on-a-chip that can be used to investigate the human urethra up close and find ways to regenerate healthy urethral epithelium after development of a stricture. One of the unique characteristics of the urethral environment is the intermittent flow of fluid that the tissue experiences from urination and ejaculation. This kind of force from fluid has been shown to affect the shape and behavior of cells in other tubular organs, and previous studies in our lab have investigated whether constant flow causes cells to look different when compared to no flow at all. However, no one has looked into whether there is a difference in the effects of life-like intermittent flow compared to constant flow or compared the results directly to a real urethra. The goal of the research described in this report was to find out whether this change in flow pattern affects the way urethral epithelial cells look, and specifically whether they become more similar to cells that can be seen in dissected tissue.

Several testing methods were used to find these answers. A programmable pump was used to expose pig urethral cells grown in the lab to the two different patterns of flow, and after three days under each condition, the shapes of the cells were looked at, including cells that experienced no flow as a reference. In order to compare these cells to the real urethra, a pig penis was dissected such that the shape of the cells on the urethra could be visualized under a microscope. Two aspects of cell shape were compared, the first being how elongated the cell was and the second being to what extent the cell was pointing in the direction that the flow was going. It was hypothesized that the cells exposed to intermittent flow would be most similar to the real urethral cells in comparison to those exposed to constant flow and to no flow, however this was not the case. The intermittent

flow led to the most elongated cells, whereas the cells in the real urethra were more a more regular shape, and the cells in all conditions were mostly pointed in random directions.

Some beginnings were made that will allow the measurement of how these cells function at the molecular level. This will give even more answers than just looking at their shape, but these experiments have not yet reached the final stage. It would also be useful to do these same experiments on buccal epithelial cells to see how good of a substitute for urethral cells they really are. All in all, it wasn't shown that urination-like flow causes lab-grown urethral cells to look more like urethral cells still connected to the penis. When creating a urethra on a chip, other characteristics will need to be included beyond the flow pattern to direct the cells towards the desired urethral behavior.

3   Contents

4 Introduction

4.1 Urethral stricture disease

Although little talked about, diseases of the urethra affect millions of men around the world. There are varied pathologies that have different prevalence and severity, from cancer to congenital disorders. One of the most common afflictions of the urethra is urethral stricture disease (USD), which presents as a fibrous obstruction of the urethra making it difficult and painful to urinate and ejaculate.[3]
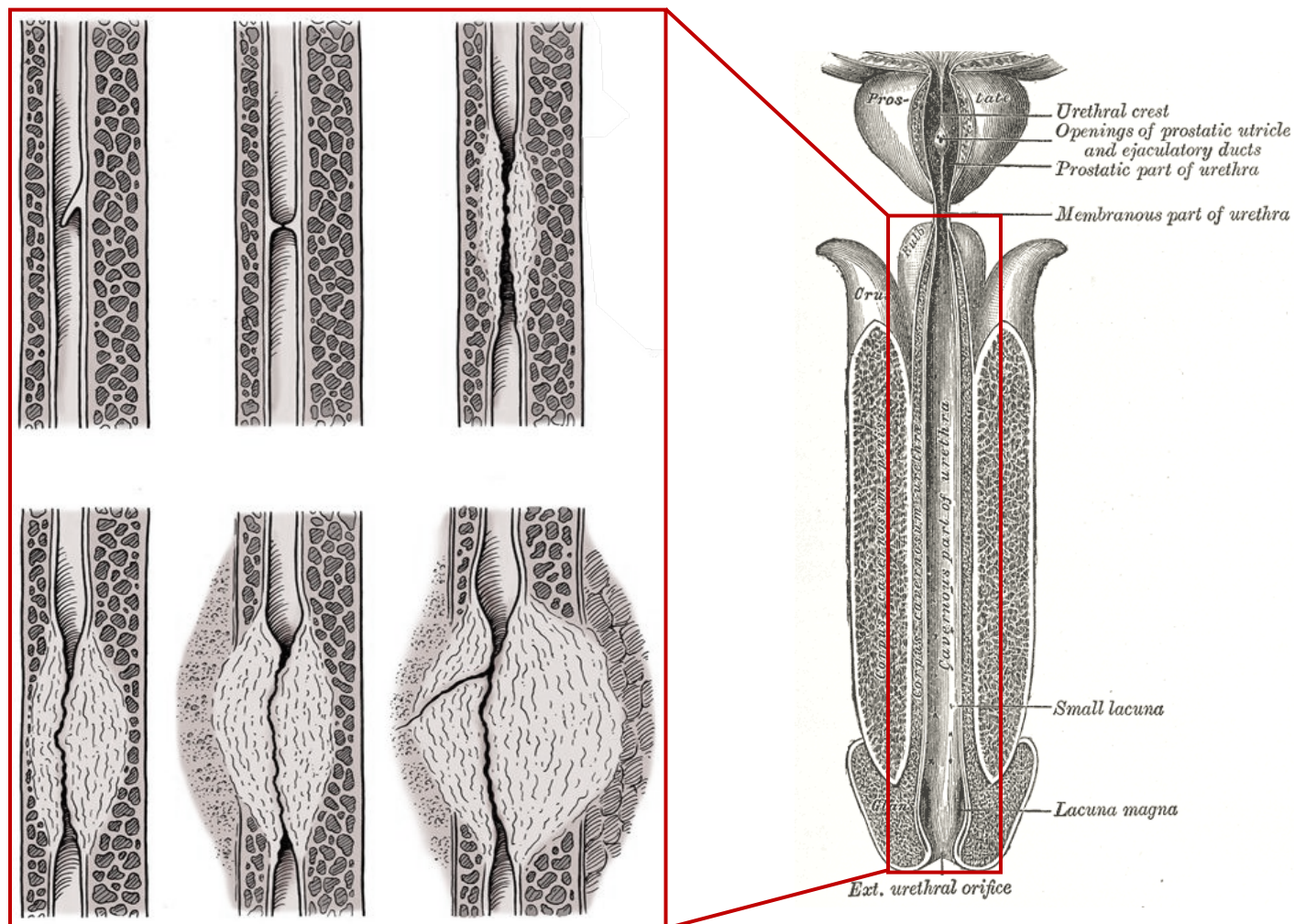

Figure 1: Anterior urethral strictures occur in the urethra from the tip of the penis to the apex of the prostate. They involve the obstruction of flow through the urethra due to fibrous tissue growth of varying severity.[4,5]

As in other soft tissues, this fibrosis often develops during a wound-healing process triggered by an injury, which can be idiopathic, congenital, iatrogenic, traumatic, or inflammatory in origin.[6] The most common causes of urethral injury are catheterization and endoscopy[7], procedures which are performed in hospitals on a daily basis. They can also occur from the treatment of other urological conditions, including hypospadias, a congenital malformation of the urethral meatus occurring in 1 out of every 600 males born in the Netherlands.[8]

Current clinical treatments for USD depend on the severity of the stricture. A fibrotic area of less than 2cm can often be treated by excision of the area followed by end-to-end anastomosis, whereas a larger defect necessitates the use of a graft or flap. For several years, the gold-standard for urethral grafting is the buccal mucosa, harvested from the interior of the patient's own cheek (Figure 2). The buccal area is easy to access, quick to heal, and has a wet environment, like the urethra, making it the first choice for urologists. That said, both techniques have downsides as well. There is a greater risk for penile shortening and curvature following an anastomotic correction versus use of a graft since tissue is only removed with none added in its place.[2] Grafting requires harvesting, which has the typical complications of donor site morbidity and imperfect compatibility with the recipient tissue.

While often not life threatening, USD and other penile diseases can have a great impact on patients' quality of life. It has been reported that as many as 70% of men who develop USD experience lower urinary tract pain, along with sexual dysfunction, abnormal voiding patterns, and recurrent urinary tract infections. Although the pain resolves in the majority of patients post-urethroplasty, quality of life is also affected by the manifestation of negative psychosocial influences. A majority of men experiencing USD and urethroplasty experience anxiety and depression that decreases with improved urinary symptoms.[9] Beyond effects on patients, Brandes, et al. showed that USD has a significant and lasting impact on the families and loved ones of USD patients, reporting a reduction in sleep, social interactions, and sexual intimacy.[10] These far-reaching consequences make investigation of regenerative USD solutions all the more relevant.
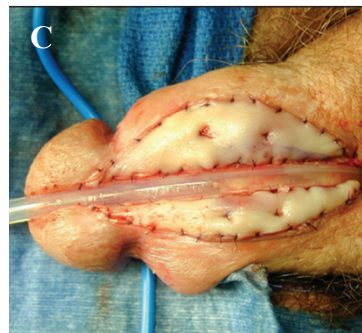

*Figure 2: Buccal mucosa is harvested (**A-B**) from the patient's cheek. The graft is sewn in place before closing the urethra (**C**).[1,2]*

4.2   Previous regenerative research

Ideally, the same tissue that was lost would be regenerated so that it could integrate seamlessly into the native environment and not require additional surgery on another organ. This goal is what has led to urological research in the field of regenerative medicine, including that which is described in this report, which could ultimately lead to solutions for the problems now faced by patients, doctors, and families dealing with USD.

Because surgery is traumatic, costly, and involves the risk of further injury or complications, the reversal of fibrosis by less invasive means would be preferred. The cure for fibrosis is something highly sought after in all fields of regenerative medicine, and there are still many challenges to overcome before fibrosis is fully reversible.[11] In general, prevention of fibrosis is much more achievable and the efficacy of local therapies for the reduction of urethral stricture recurrence has been reviewed. Although several pharmaceutical treatments showed promising results, a lack of long-term follow-up still leaves questions as to their clinical efficacy.[12] Additionally, since 1 USD case out of 3 is considered idiopathic[7], prevention is not a possibility for a large patient population.

Many biomaterials and tissue engineering approaches have been explored for use in surgical urethral reconstruction, and several of these studies follow the same general approach. The first step is to obtain a scaffold to mimic the urethra's own extracellular matrix (ECM), through techniques including electrospinning[13], decellularization of autologous[14] or xenogeneic[15] epithelium, and tubularization of polymer mesh.[14] This scaffold can then be infused with urethral epithelial cells and grown out in-vitro or left bare. The newly created urethral graft can then be implanted through standard grafting techniques. Positive results were presented in many of these studies, with optimistic conclusions for the translatability of the respective techniques. However, there is again a lack of long-term follow-up for adult sufferers of anterior USD.

Beyond urethral cells, researchers have investigated the development of tissue engineered buccal mucosa grafts for use in urethroplasty. Bhargava, et al. described a clinical study in patients requiring "extensive substitution urethroplasty," which involved the grafting of decellularized cadaveric scaffolds seeded with oral fibroblasts and keratinocytes. This was shown to be somewhat successful; three out of five patients had usable results after nine years, though some moderate interventions were still needed in all cases.[16] The same techniques described for urethral reconstruction could conceivably be used for engineering buccal mucosa grafts. This may be preferable since they are a much more readily available tissue type and therefore merit further investigation as a cell source for urethral regeneration.

4.3   Urethra-on-a-chip

There is agreement within the field of urology that more basic science is needed to elucidate the physiology and mechanistic functioning of the urethral mucosa before true success can be achieved in tissue engineering urethral tissue for clinical use.[17] Although animal models, commonly rabbits or canines, have been used for urethral research, they don't adequately recapitulate the unique anatomy and molecular environment of the human penis.[18] Not only that, but it may be argued that it is irresponsible and unethical to proceed with in-vivo experiments before adequate fundamental knowledge has been gained.

More and more fields within regenerative medicine that face the same challenges have been turning to organs-on-a-chip (OOCs), microfluidic devices that can recapitulate the relevant physiological characteristics of an organ of interest. In this way, cell behavior, drug efficacy, molecular interactions, and more can be studied in an in-vitro system that's well-controlled and far more clinically relevant than 2D culture.[19] In this study, one step was taken towards an ultimate goal of developing a urethra-on-a-chip for the closer study of urethral epithelial function, pathophysiology of fibrosis, and eventual urethral tissue engineering.

A significant challenge in designing an organ-on-a-chip is deciding which combination of the innumerable environmental influences a tissue experiences in the body will achieve a simple yet accurate in-vitro model. There are two main types of stimuli that influence cell phenotype: mechanical and chemical. Chemical stimuli are nearly impossible to list fully for any cell type, as they come from other organs through the blood, other cells through the ECM, and even the outside world in the case of the urethra. For this reason, the research in this report focuses on the relevance of mechanical factors in urethral epithelial phenotype. For urethral epithelial cells, mechanical stimuli include fluid shear stress experienced during urination and ejaculation, cyclical strain that occurs during erection and in the presence of fluid pressure, and direct cell-cell and cell-basement membrane interaction. Fluid shear stress has been investigated in this lab previously, though cell were only exposed to constant flow, which is not physiologically accurate, or stress levels that did not match up with those occurring in the body.[20-22]

It's hypothesized that the more similar the OOC environment is to the native urethra, the closer the behavior of the cultured cell will be to those in-vivo. The overall goal of this research is to narrow down which attributes of the native urethra are relevant for inclusion in a urethra-on-a-chip. The specific aim is to investigate whether exposing urethral epithelial cells to a flow pattern and fluid shear stress simulating urination directs the cells towards a more physiological phenotype when compared to unchanging flow or no flow at all. A secondary aim of this research is to investigate how buccal mucosa compares to urethral cells and tissue when exposed to the same conditions. By comparing the morphological characteristics of urethral cells in tissue and cells cultured under intermittent, constant, and static flow conditions, these aims were pursued.

This report's goal is to describe the purpose and process of each step of this study in a clear and readable manner, to better serve future researchers endeavoring to continue this ongoing exploration, as well as other interested parties.

5 Materials and Methods[†]

5.1 Cell culture

5.1.1 *Primary porcine urethral epithelial cells (pUECs)*

pUECs were previously isolated from urethral biopsies of adult boars (*Sus scrofa*) at UMC Utrecht and stored in liquid nitrogen. Frozen cells were plated onto culture plastic coated with gelatin by incubating with a 0.1% w/v solution in phosphate-buffered saline (PBS) at 37°C for 10 minutes. Medium used was Urothelial Cell Medium (UCM) including supplements (ScienCell) with 5% Fetal Bovine Serum (FBS) (Gibco), added as recommended for adherent cell culture. Cells were passaged using 0.05% Trypsin-EDTA, phenol red (Gibco) in a 1:2 ratio at 90% confluency. Centrifugation of cells was done at 1000rpm for 5 minutes at 4°C.

5.1.2 *Primary human buccal mucosa cells (hBMCs)*

hBMCs were previously isolated from biobank-stored biopsies of a healthy 39-year-old male urological patient (ID: hBM SF20-218) and stored in liquid nitrogen. Cells were treated similarly to the pUECs, the exceptions being that the culture medium used was Oral Keratinocyte Medium (OKM) including supplements (SceinCell) with no FBS. Accutase solution (Sigma-Aldrich) was used as the cell detachment solution.

5.1.3 *Medium Optimization*

An experiment was done to determine which medium was to be used for experiments in which pUECs and hBMCs were exposed to the same conditions. Both cell types were seeded into 6 wells each of a 12-well plate and were allowed to attach in their preferred medium for 24 hours. After this, one well of each cell type had their medium changed to UCM, OKM, or a 1:1 mixture of UCM:OKM, each with and without 5% FBS. After 72 hours, the cells in their preferred medium were visually compared to those in each varying condition.

5.2 Flow experiments

There were two treatment groups in the flow experiments, cells experiencing either a Constant or Intermittent Flow state. The control group consisted of cells experiencing No Flow.

[†] All standard chemicals were obtained from Sigma-Aldrich.

For all flow experiments, the ibidi Pump System (Figure 3) was used to expose fluid shear stresses to cells in the treatment groups. Six-channel microslides, ibidi μ-Slide VI$^{0.4}$, with channels connected in series using the associated serial connector tubes, housed the cells and were used in combination with the ibidi Red Perfusion Set. Official protocols for ibidi products were followed. All materials were pre-warmed to 37° prior to each experiment to minimize the chance of bubbles forming once the fluid system is closed. μ-Slides were coated with gelatin as described above, seeded with cells at a density of $3*10^6$ cells/mL, and left at 37° under static conditions for 24 hours. μ-Slide channels were then connected in series, the slide was attached to the Perfusion Set, and the flow program was initiated from the connected computer and pump.
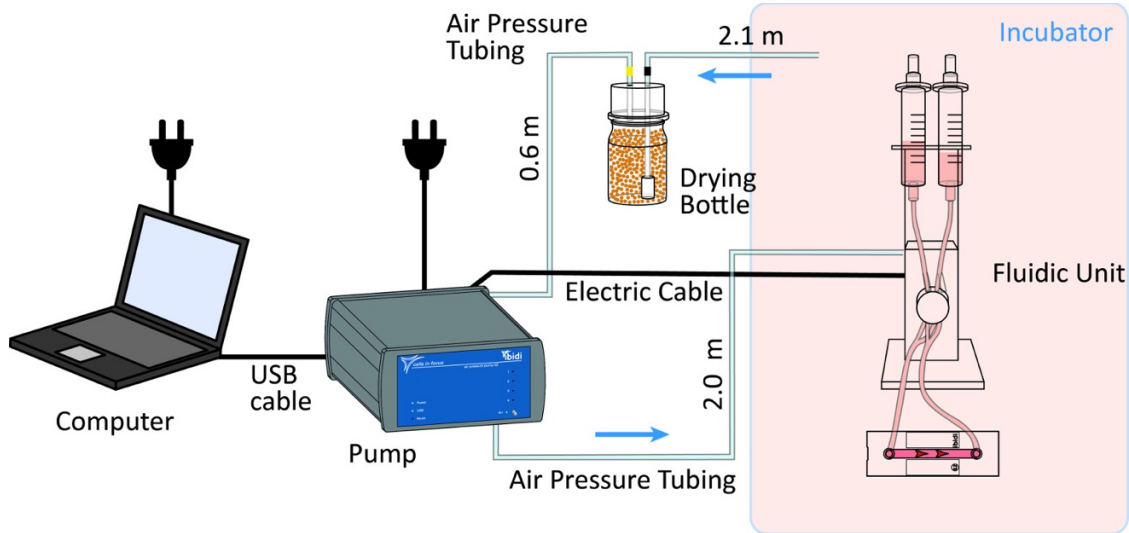

Figure 3: The ibidi Pump System, featuring a single-channel slide. The Fluidic Unit incorporates a valve which actuates the tubing of the Perfusion Set to enable unidirectional flow through the μ-Slide. Positive air pressure is provided by the pump outside the incubator, the pattern of which is determined by the program set by the user in the attached computer. A tube and cable connect the Fluidic Unit to the pump through the door of the incubator.

The maximum shear stress to be applied to cells was calculated based on the maximum flow rates seen in urination among healthy males[22], the viscosity of the UCM, and the approximate diameter of the male urethra.[5,23] Using Equation 1, a maximum shear stress of 9.2dyn/cm² was found.

$$\tau_{max} = \frac{4\mu Q_{max}}{\pi r^3}$$

$$9.2\frac{dyn}{cm^2} = \frac{4*0.008\frac{dyn*s}{cm^2}*\frac{31mL}{s}}{\pi*(0.325cm)^3}$$

Equation 1: This equation can be used for determining shear stress in a tube. It relies on the assumption that the urethra is straight and cylindrical, and that the flow within is laminar.[24] t is shear stress (dyn/cm²), m is viscosity in (dyn•s/cm²), Q is flow rate (mL/s), and r is radius (cm).

Both treatment groups involved gradual increases in shear stress up to p$_{max}$ at the start of flow to acclimate the cells to fluid shear. After this period, the Constant Flow group maintained

this shear stress for the 72-hour experimental period. Conversely, the Intermittent Flow group was exposed to long periods of near-static conditions (shear stresses less than $0.1 dyn/cm^2$) interrupted by short bursts of flow, timed so that they occurred approximately 7 times per 24-hour period, mimicking urination.[25-27]

A. Constant Flow pressure levels over a 3-day experiment
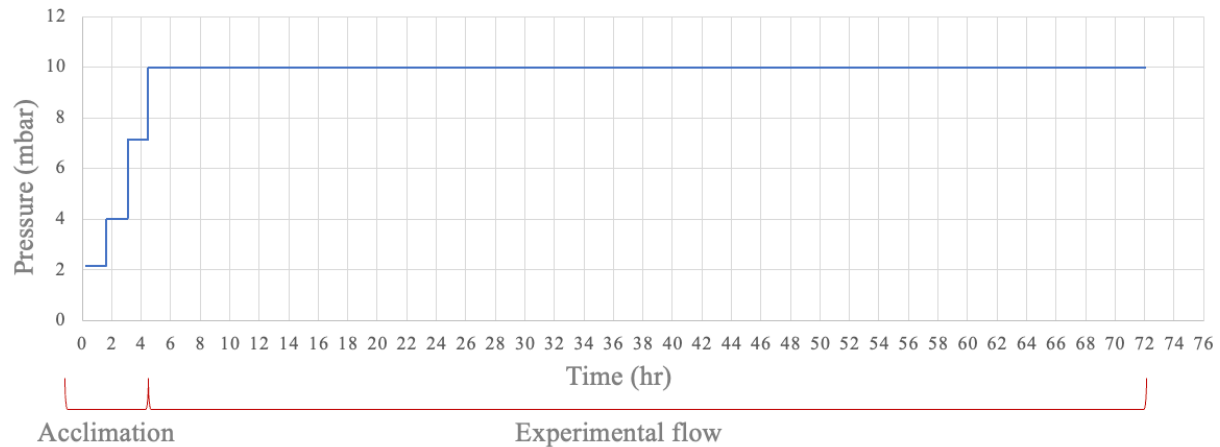
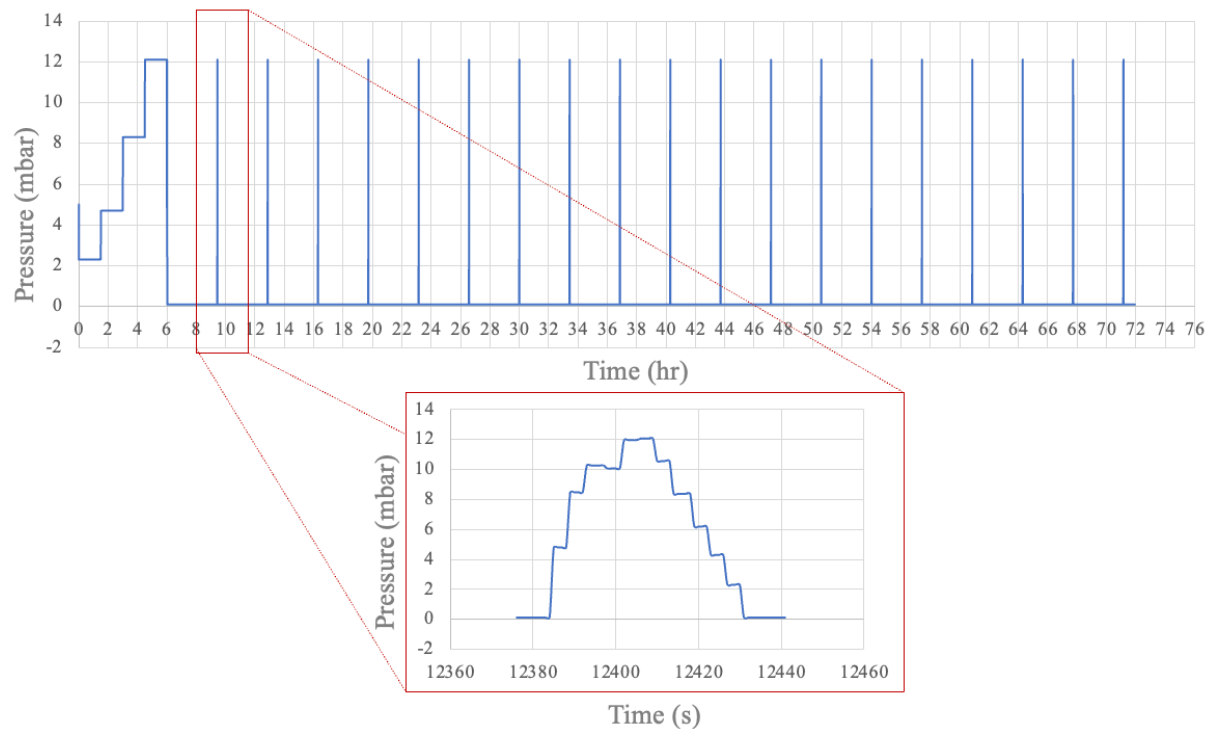**B.** Intermittent Flow pressure levels over a 3-day experiment

Figure 4: Both graphs show the same acclimation period, involving steps of 2, 4, 7, and 9.2dyn/cm² for 90 minutes each. A depicts the variation in pressure, or lack thereof, during the course of a Constant Flow treatment. B depicts the Intermittent Flow treatment's 44-second patterns of flow, modeled after healthy uroflowmetry data, in between the 206-minute periods of stasis. In both graphs, the maximum pressure corresponds to 9.2dyn/cm². Pressures needed to induce certain

shear stresses were calculated automatically by the ibidi Pump Software based on the flow rate calibration factor, which varied.

Cells in the No Flow group were also seeded onto µ-Slides, but the channels were not connected in series, nor was the slide attached to the pump system. Medium was changed 24 hours after seeding cells in all flow conditions and every 24 hours for the No Flow group. For the Constant and Intermittent Flow groups, additional medium was added to the pump system if there was a fluid loss of 1mL or more.

For all flow conditions, the experiment ended 96 hours after cell seeding. Three channels of the 6-channel µ-Slides were fixated for immunofluorescent staining, and the cells in the remaining three were harvested and combined for use in RT-qPCR.

5.3 Reverse transcription-quantitative polymerase chain reaction (RT-qPCR) assays

pUECs and hBMCs were processed for RT-qPCR assays. RNA isolation was done with the ISOLATE II RNA Mini Kit (Bioline), which produces 30mL of RNA, and quality was assessed using a DeNovix DS-11 Spectrophotometer. Complementary DNA (cDNA) synthesis was done with the SensiFAST™ cDNA Synthesis Kit (Bioline) so that 500ng of cDNA was produced in a 20mL solution. The same cDNA synthesis procedure was performed without the use of reverse transcriptase to produce no reverse transcriptase (NRT) controls, which can inform about the presence of genomic DNA contamination.[28] RNA and cDNA were stored at -20°C.

Gene expressions measured via this assay were to include the genes that code for the proteins Zonula Occludens-1(ZO-1), Uroplakin II (UPII), Mucin 4 (MUC4), and Claudin 3 (CLDN3), all of which could be used to characterize an aspect of urethral epithelial functionality.[29-33] Glyceraldehyde 3-phosphate dehydrogenase (GAPDH) was also included, which is frequently used as a reference gene due to its ubiquitous expression in mammalian cells.[34] Primers for these genes were designed by combining a protein-coding sequence found in Ensembl[35] for the *S. Scrofa* genome with the Primer-BLAST tool by NCBI.[36] Primers were ordered from Sigma-Aldrich, resuspended in pH 7.5 TE buffer to 100mM, and stored at -20°C. Multiple primer pairs were ordered for each target gene to increase the chances of having at least one pair with usable efficiency. Specific details can be seen in Appendix
Supplementary Table 1.

5.3.1 Primer efficiency testing

Efficiency testing was done for each newly designed primer pair. FastStart Universal SYBR Green Master (Roche) was used as the fluorophore, which comes at 2x concentration. Each 20mL well of the PCR plate contained a primer concentration of 0.3mM (~0.4mL) for each the forward and reverse primer, a sample amount of 1mL, and a SYBR Green Master amount of 10mL, with the remaining volume occupied by DNase-free water. The 1mL sample volumes consisted of cDNA at a 5ng/mL, 0.5ng/mL, 0.0.05ng/mL, or 0.005ng/mL concentration for each primer pair. A 1mL sample of NRT with a concentration of 5ng/mL and a no template control (NTC), in which the 1mL cDNA sample volume is replaced with DNase-free water, were also present for each primer pair. An example of how this would be laid out on a PCR plate is shown in Figure 5. The

plate would then be run in a CFX96 Touch Real-Time PCR Detection System (Bio-Rad) using a thermal cycling protocol as specified in Supplementary Figure 1.

Primer pair efficiency could be quantified from the data produced by the PCR Detection System. For a given primer, the quantitative cycle (Cq) value was given at each cDNA concentration. These four Cq values were plotted against the negative logarithm base 10 of the respective cDNA concentration, and the slope of the resulting linear regression was input into Equation 2 to obtain the primer pair's efficiency.

$$Efficiency\ (\%) = \left(\frac{-1}{10^{Slope} - 1}\right) * 100$$

Equation 2: Calculation of primer efficiency based on the slope of a standard curve.[28]

Figure 5: An example of how a PCR plate could be arranged to test primer pair efficiency based on serial dilutions of cDNA. Cells outlined in orange contain negative control samples, either NRT or NTC, while the rests contain cDNA samples. A primer pair that is known to have a high efficiency should be included, in this case GAPDH (yellow outline), as a positive control.

5.3.2   Temperature gradient qPCR

Gradient qPCR was done with primer pairs that exhibited low efficiency in order to determine whether there was a more optimal annealing temperature that could lead to high efficiency. The primer pairs used in these experiments were CLDN3 (P7), MUC4 (P8), UPII (P9), ZO-1(P23), and GAPDH (PdG 5/6). The protocol involved a similar setup to the standard curve primer efficiency tests, the difference being that the annealing temperature varied within each primer instead of the cDNA concentration. Thermal cycling using eight annealing temperatures, from 53°C to 63°C, was done on one well from each primer (details shown in Figure 6 and

Supplementary Figure 2). As such, the well composition was the same for the non-control wells within each primer: 10mL SYBR Green Master, 0.3mM (~0.4mL) for each the forward and reverse primer, 1mL of cDNA at 1ng/mL, with the remainder of the 20mL volume occupied by DNase-free water. An additional column of the GAPDH primer pair was used for NTCs, in which the cDNA volume was replaced by DNase-free water. The optimal annealing temperature for a given primer pair was determined to be that at which the lowest Cq value was obtained.

Primers that still showed little or no DNA amplification were also put through the UCSC In-Silico PCR (isPCR) program[37], which outputs any genomic segments that fall between the input primer pair. If no match is found, this could suggest that the primer pair is not finding its DNA target.
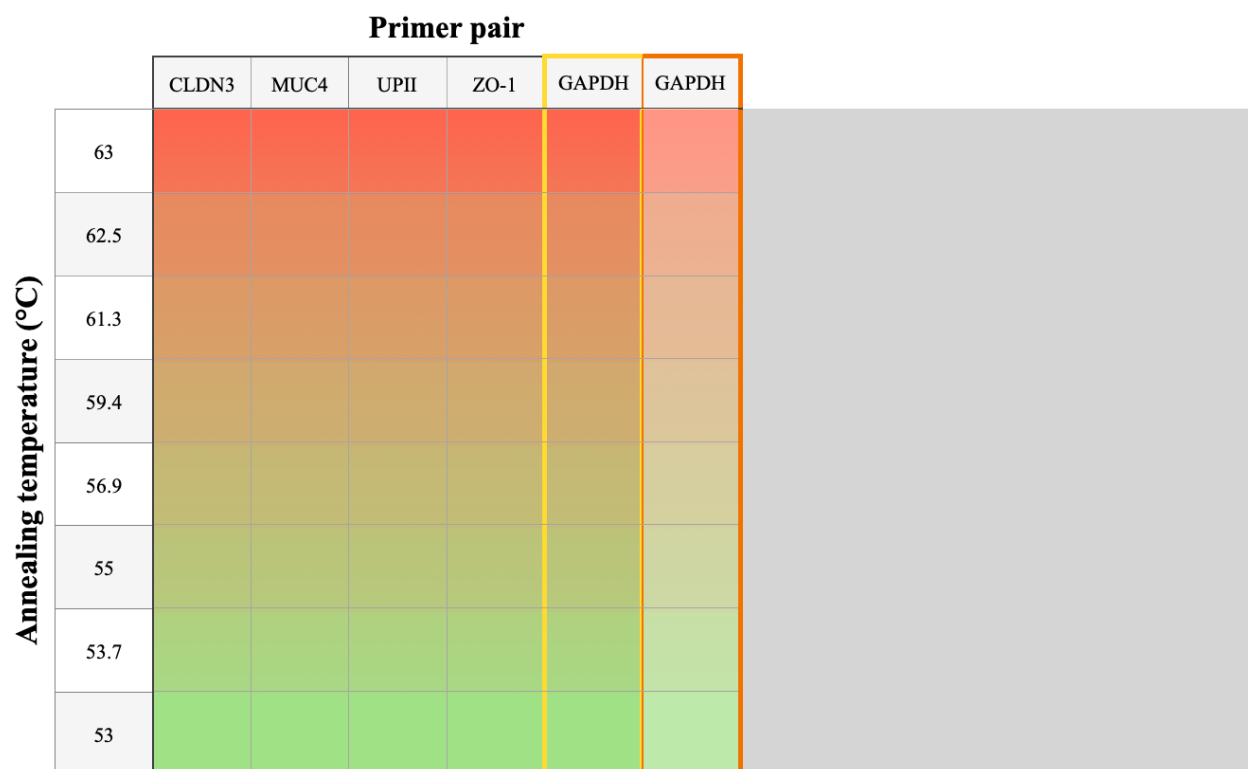

Figure 6: An example of how a PCR plate could be arranged to test a gradient of annealing temperatures on multiple primer pairs. NTC wells are outlined in orange and positive control wells are outlined in yellow.

5.4 Tissue dissection

An unpreserved, juvenile pig penis was obtained from UMC Utrecht. The penis was dissected first longitudinally to expose the urethra, then cross sectionally to isolate proximal segments, and then longitudinally again to obtain two penis pieces of one-half circumference from each segment.
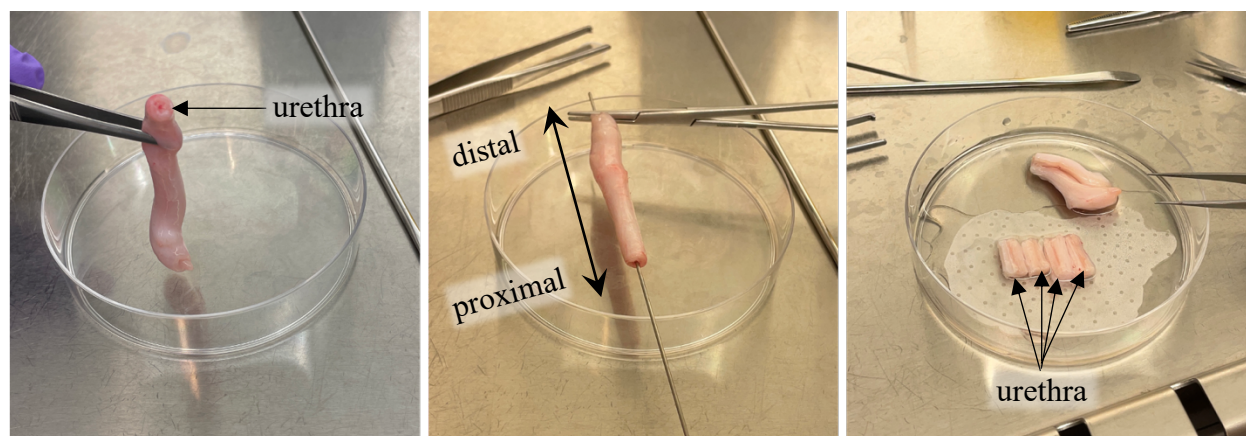
Figure 7: The distal end of the porcine penis displayed a corkscrew-like shape, so the proximal end was harvested for best urethral visualization.

5.5   Immunostaining and fluorescent microscopy

5.5.1   *Microfluidic slide (μ-Slide) staining*

μ-Slide VI$^{0.4}$ microfluidic slides (ibidi) were prepared for immunocytochemical (ICC) fluorescent staining by filling the channels with 1% formalin, or 0.37% formaldehyde, and incubating at room temperature for 20 minutes. Channels were then filled with PBS and stored at 4°C until immunofluorescent staining was performed. At that time, cells in each channel were permeabilized with 0.05% TritonX (TX)-100/PBS for 15 minutes, then blocked with 2% Bovine Serum Albumin (BSA) in 0.01% TX-100/PBS for 30 minutes. Primary antibodies rat anti-ZO-1 sc-33725 (Santa Cruz Biotechnology) and mouse anti-human cytokeratin-7 (CK-7) M7018 (Dako) were diluted 1:100 in blocking solution and incubated with the cells at room temperature for 2 hours. Cells were washed three times with 0.01% TX-100/PBS in 5-minute intervals. Secondary antibodies Alexa Fluor 555 (AF555) goat anti-rat and Alexa Fluor 488 (AF488) goat anti-mouse (Invitrogen) were incubated with cells for 1 hour at room temperature at a dilution of 1:600 in blocking solution along with DyLight 488 Phalloidin 12935 (Cell Signaling Technology), diluted 1:40 from a 40X stock. Cells were again washed three times for 5 minutes per wash following this incubation, then incubated at room temperature for 5 minutes with 4,6-diamidino-2-phenylindole (DAPI) solution (Roche) diluted 1:5000 in PBS from a 5mg/mL stock. Cells were rinsed three times with PBS, and all liquid was removed from the channels by tilting the slide and absorbing with a wipe. Channels were then filled with Fluoromount-G Mounting Medium (ThermoFisher), slides were left to set at room temperature for 30 minutes, and then stored flat at 4°C until imaging. Imaging was performed within a week of staining on a Zeiss LSM700 confocal microscope. Three images from each pUEC μ-Slide were used for data collection. They were taken at a random location along the length of the slide and were assumed to be representative samples.

5.5.2   *Paraffin-embedded tissue section staining*

Paraffin sections were created from segments of distal urethra (Figure 7) that were dissected as described above. The segments were stored in 10% formalin for about four days until tissue processing, for which the segments were placed into tissue cassettes and subject to a standard overnight tissue processing protocol. Tissue segments were then embedded in paraffin so that the urethra was facing opposite the cassette. Sections were made from a more proximal penile segment on a rotational microtome in 3mm deep slices. Slices chosen for adherence to a glass slide were at

a depth that appeared to maximize intersection with the urethral epithelial plane. Each slide contained three sections that were separated by 10-slice increments so that multiple depths were able to be seen on each slide.

A hematoxylin and eosin staining was done on one slide to assess that the slices had been made deep enough to visualize the epithelium. Deparaffination was done via a 7-minute soak in Histo-Clear (National Diagnostics) followed by a series of five additional Histo-Clear washes. Rehydration was done via a series of five 100% and one 70% ethanol water washes followed by thorough rinsing with deionized (DI) water. The rehydrated slide was dyed in hematoxylin solution for 5 minutes, rinsed under running tap water for 10 minutes, dyed in eosin solution for 30 seconds, and rinsed in DI water. Dehydration was then done via the reverse of the rehydration and deparaffination procedures, and Eukitt mounting medium (Sigma-Aldrich) was used to attach a glass coverslip. Visualization was done on a Leica DM750 microscope.

Immunohistochemical fluorescent staining of the remaining paraffin sections was performed. Deparaffinization and rehydration was done as described above, the sections were blocked in a 5% hydrogen peroxide/PBS solution for 20 minutes at room temperature, and they were then rinsed with 0.05% PBS-Tween 20 (PBS-T). Antigen retrieval was done in 1mmol/l tris/ethylenediaminetetraacetic acid (EDTA) buffered to pH 9.0 with 5N hydrochloric acid (HCl) for 40 minutes at 90°C, and after the slides were allowed to cool, they were rinsed for 15 minutes in running tap water and three times with PBS-T. The slides were blocked with 2% BSA/PBS, incubated for 60 minutes with ZO-1 and CK-7 primary antibodies diluted 1:100 in 1% BSA/PBS, rinsed three times with PBS-T, incubated for 30 minutes with AF555 goat anti-rat and AF488 goat anti-mouse secondary antibodies diluted 1:600 in PBS, rinsed three times with PBS, incubated 5 minutes with DAPI diluted 1:5000 in PBS, rinsed thoroughly with PBS, dried, and then mounted with Mowiol onto glass coverslips. Slides were stored at 4°C and images were taken within 7 days on an Olympus BX51 microscope.

5.6   Scanning electron microscopy (SEM)

One proximal penile segment, dissected as described above, was initially fixed in 10% formalin for 15 minutes and then in ice-cold 1% glutaraldehyde for 15 minutes, rinsed twice in PBS, and stored in PBS at room temperature. Dehydration of the tissue involved soaking for 30 minutes periods in 10%, 25%, 50%, 70%, 90%, and 100% (x2) subsequent concentrations of ethanol in water, 1:1 ethanol/hexamethyldisilazane (HDMS) and 100% HDMS. The tissue was then dehydrated in a vacuum overnight, mounted urethra-up to a standard pin stub with conductive tape, and sputter-coated with 10nm of gold.

Images of the urethral epithelium were taken on a Phenom Desktop SEM (Thermo Fisher). Four images used for data collection were taken at a random location along the length of the urethra and were assumed to be representative samples.

5.7   Image processing and data collection

Urethral epithelial cell images from the pUEC μ-Slides involved in flow experiments and the SEM-prepared tissue sample were used for data collection. Three pUEC μ-Slide images of each flow condition and four SEM images were processed, thirteen in total.

All processing was done in Fiji.[38] The contrast and brightness of an individual image was manipulated for optimal visualization of cell borders. In the 'Set Measurements' window, 'Fit ellipse,' 'Add to overlay,' and 'Display label' were selected. Using the 'Freehand selections' tool, every cell in the image with a distinguishable and complete border was traced, followed by calling

the 'Measure' command. For each cell, the lengths of the major and minor axes (pixels) and the angle of the major axis with respect to horizontal (°) was measured through this process (Figure 8). After all cells in an image were traced and measured, the values in the 'Results' window were saved.
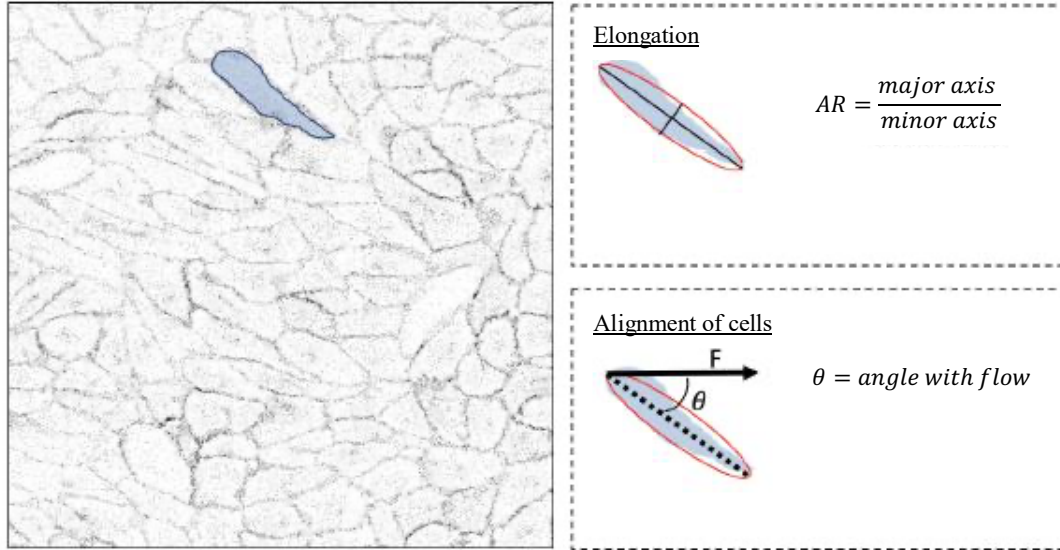

Figure 8: Tracing in FIJI and fitting an ellipse to obtain quantitative elongation and alignment data for individual cells in a monolayer (Gabriëlla Fisher, MSc, unpublished report, 2020[21]).

5.8 Data processing and statistical analysis

All data processing and statistical analysis was performed in Microsoft Excel. Elongation ratio for each cell was calculated by dividing the major axis length measurement by the minor axis length measurement (Figure 8). Angles measured in FIJI for a fitted ellipse are in reference to the image's positive vertical axis by default. The direction of flow in pUEC μ-Slide images was parallel to the images' horizontal axes, so the angles measured for these images was processed by Equation 3. For SEM images, the direction of flow was parallel to the images' vertical axes, so the angles measured for these images was processed by Equation 4.

$$\theta = |measured\ angle - 90|$$

Equation 3: Calculation performed for images with a direction of flow perpendicular to the vertical axis in order to obtain an alignment angle in reference to the direction of flow.

$$if\ measured\ angle > 90°, \theta = |measured\ angle - 180|$$

Equation 4: For images with a direction of flow parallel to the vertical axis, this calculation gives an alignment angle that expresses the shortest possible angle to the direction of flow.

For statistical analysis, each cell was treated as an observation, and cells from the same condition were grouped together from multiple images. Pairwise Welch's t-tests were performed between each condition (No Flow, Constant Flow, Intermittent Flow, and Tissue) for elongation and alignment data. One-way ANOVAs were also performed within each condition to investigate the presence of significant intra-condition variability. Each test used an alpha value of 0.05 and considered a p-value below 0.05 to be significant.

Histograms were created for each condition's alignment data to visualize the angle distribution. Each bucket had a value of 1° from 0° to 90°.

6 Results & Discussion

6.1 Flow experiments

The medium optimization experiment showed that using serum with hBMCs resulted in increasing numbers of cells with fibroblast-like morphology, although there was no noticeable difference between UCM and OKM. For pUECs, there was no noticeable difference between the control medium (UCM with serum) and any other condition, so UCM without serum was used in flow experiments for both cell types.

Transmitted light images were made immediately before starting each flow experiment, at time point hour 0, and immediately after their conclusions, at hour 72, in order to visually compare the changes in individual cell morphology, monolayer formation, and intercellular interaction between different flow conditions and cell types. These images are shown in Figure 9; in all flow experiments shown, there is a clear difference between the first and final time points. Images of channels with complete or near-complete confluency by hour 0 were chosen to minimize the effect of normal cell growth on the visual differences between hour 0 and hour 72, however there were still rounded, unattached cells present in the channels at hour 0 despite having had the medium changed. Though the amount is less, some of these can still be seen at hour 72 in the No Flow channel, whereas the flow seems to have removed them from the other pUEC conditions. In the hBMC flow conditions, the presence of these rounded elements seems to have increased by the last time point, though their identity as cells in uncertain. They appear not to be living and attached cells, as they don't appear in the fluorescent images from the same 72-hour time point (Figure 10H).

In all flow-positive conditions, individual cell borders are more distinct at hour 72 than at hour 0, whereas the difference in cell borders between the two time points of the No Flow condition is less distinguishable. This suggests that cells under static conditions remain flatter than those under flow.

At the 72-hour point, μ-Slides were fixed and stained for ZO-1, beta-actin, CK-7, and DAPI (Figure 10). The morphological differences between the pUEC Intermittent and Constant Flow conditions and the No Flow condition is apparent in these images as well. Actin fibers in the cells cultured without flow (Figure 10E) seem to stay within the borders delineated by the tight junctions Figure 10A), whereas the fibers of the Intermittent and Constant Flow conditions (Figure 10F-G) reach beyond their individual cell borders and create an interwoven network across the monolayer.

Only images of the Constant Flow cells of the hBMCs were obtained, as the No Flow cells died during their experiment and the Intermittent Flow cells washed off during immunostaining. Most notably, the ZO-1 antibody is not visible in these cells. One possible reason for this is that, unlike urethral epithelium, buccal mucosa is multi-layered.[39,40] Imafuku, et al. found that ZO-1 is located in the top third of buccal mucosa tissue, which may suggest that the hBMCs isolated for this experiment may have been taken from the bottom two-thirds of the tissue which do not express ZO-1. In addition, culturing in a two-dimensional monolayer may select for basal cells since they undergo cell division, in contrast to their more apical counterparts.[41]

A lack of tight junctions between hBMCs is also supported by looking at Figure 10H, which depicts the staining of beta-actin. These actin fibers don't extend beyond the borders of their

cells of origin, resulting in an image that's much more similar to the No Flow condition of pUECs rather than the other cells under flow. Without other hBMC flow conditions to compare it to, it's not possible to say what changes were induced in the cells in response to flow, but it could be beneficial in a future experiment to investigate the phenotype of these cells and whether they could be made to form tight junctions under certain conditions.
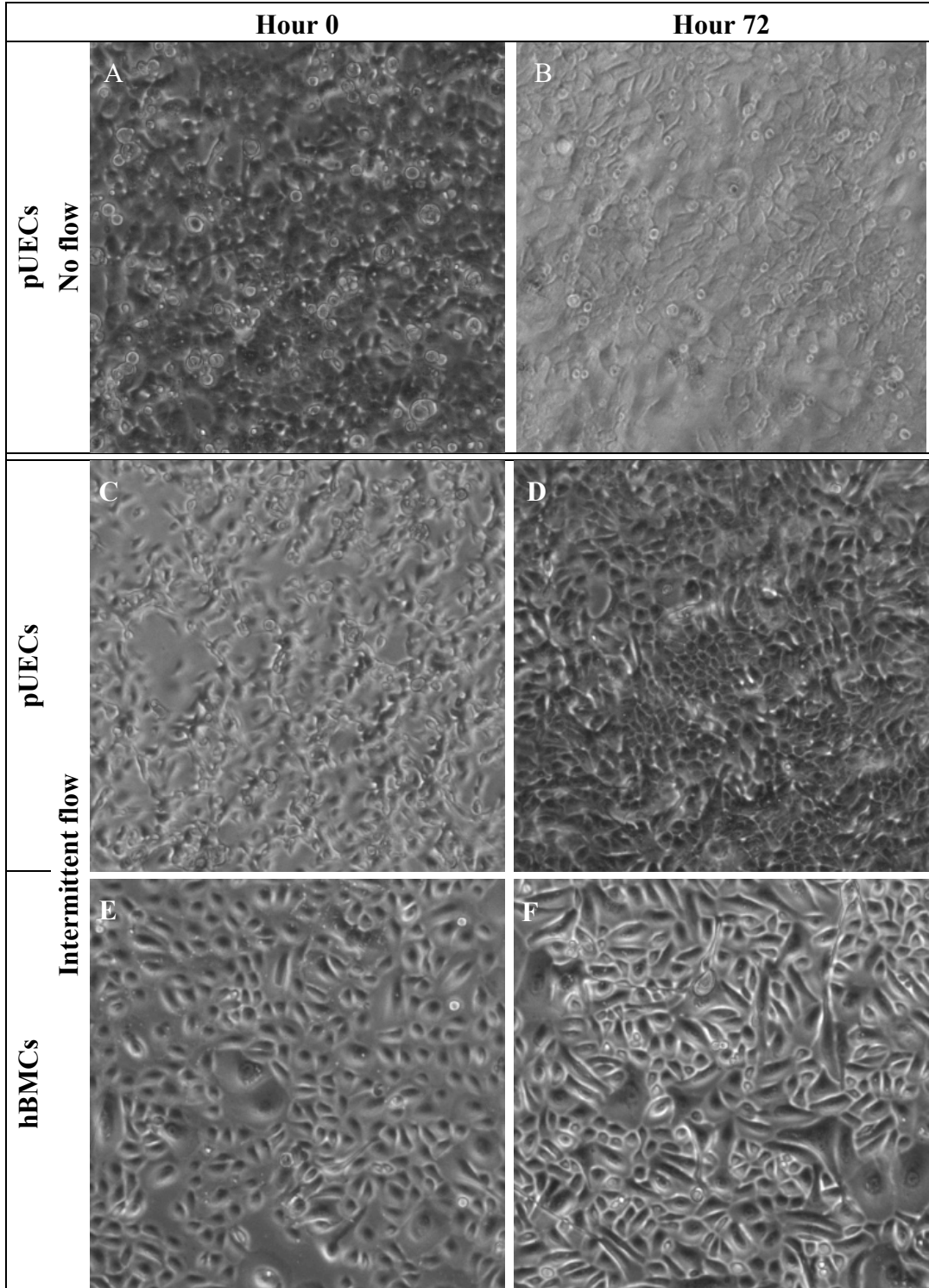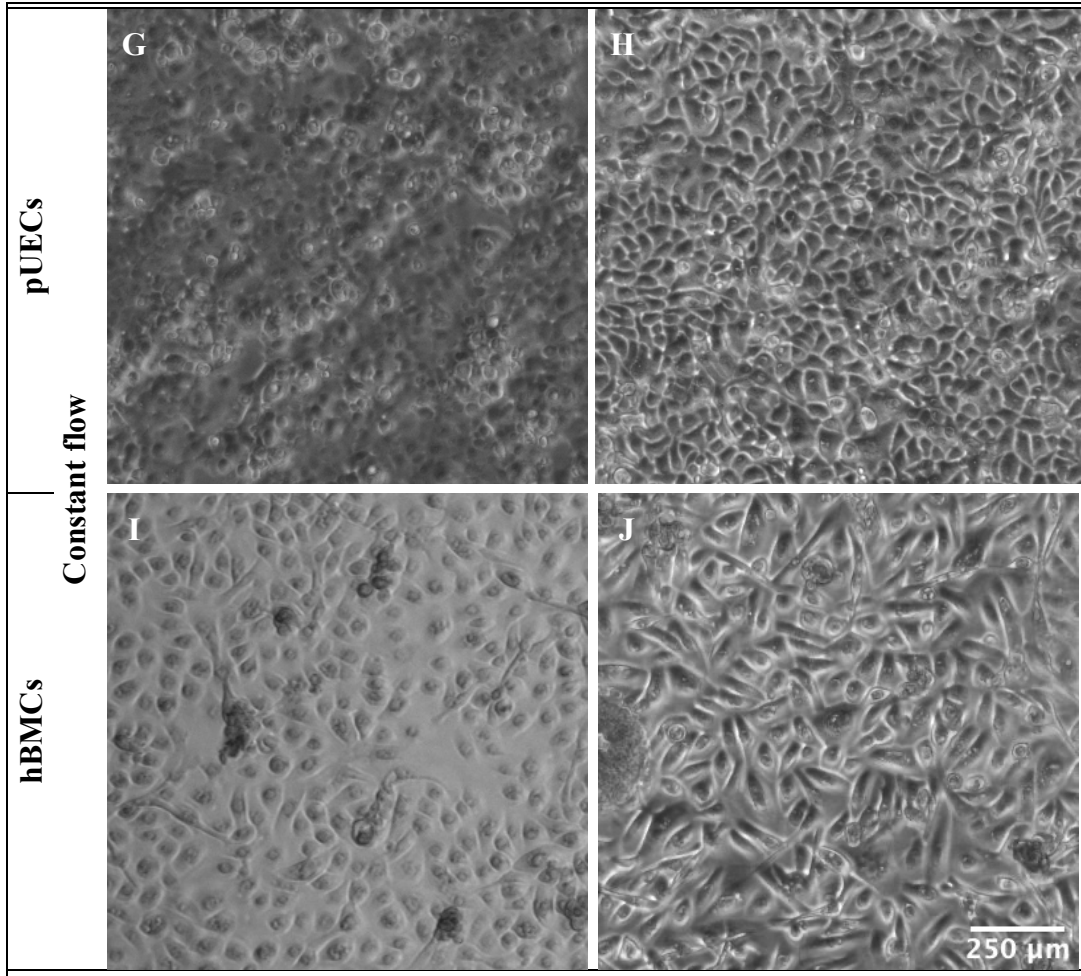
Hour 0	Hour 72

Figure 9: Transmitted light images were taken on an EVOS microscope at hour 0, the starting time point, and hour 72, the ending time point, of each flow experiment. Images from the same flow condition were taken of the same channel, but not of the exact same position on the channel. Cells were not fixed at the time of imaging.
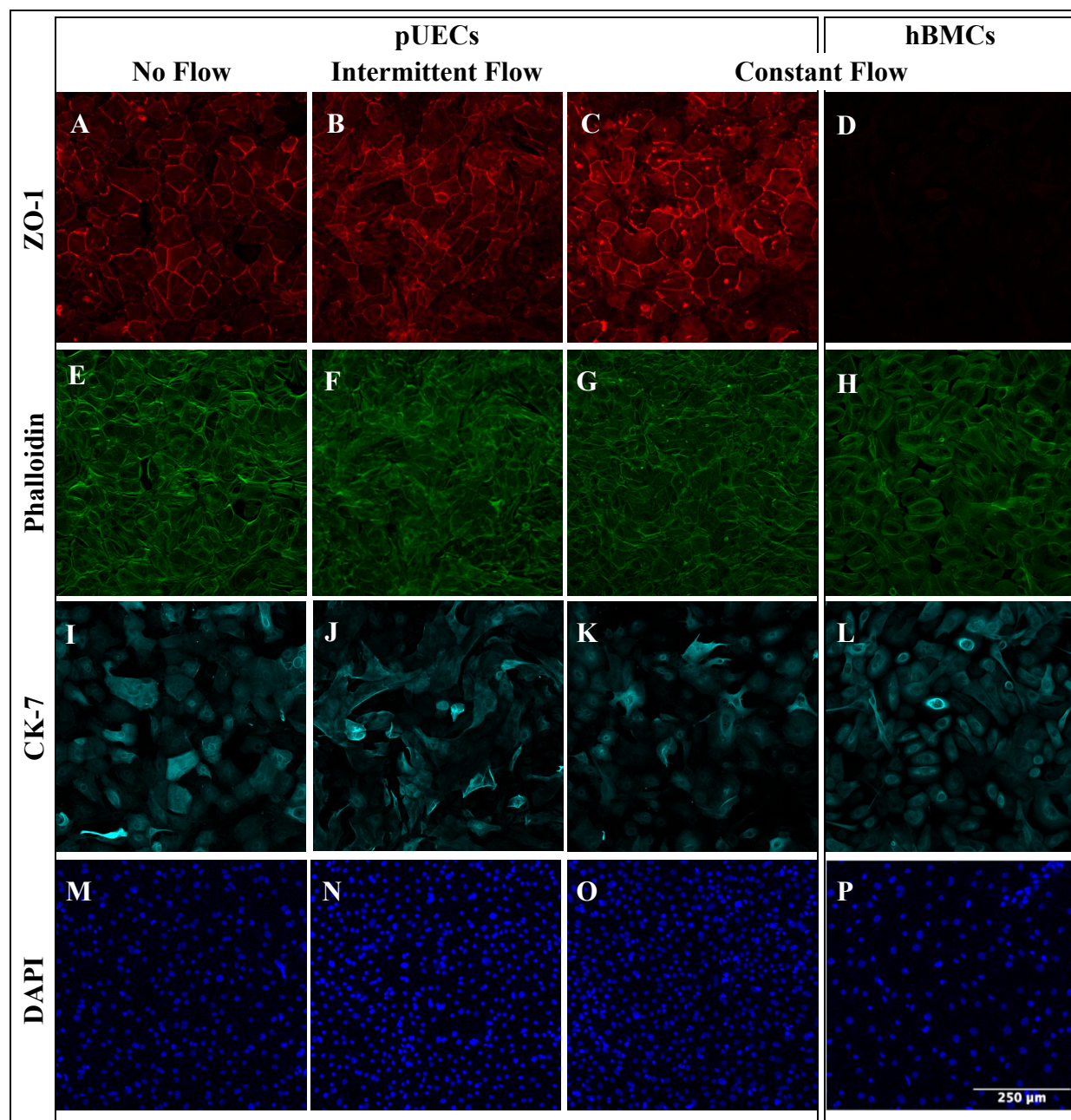
Figure 10: Cells underwent a 72-hour flow experiment, pUECs experiencing three different conditions and hBMCs experiencing two (one shown), and were then fixed and stained for ZO-1 (A-D), marking tight junctions, phalloidin (E-H), marking beta-actin, cytokeratin-7 (I-L), a cytoplasmic marker, and DAPI (M-P), which stains the nuclei. Each column of images was taken in the same location on the µ-Slide channel.

Quantification of elongation and alignment to the direction of flow was done on cells whose borders could be well visualized, and therefore only cultured pUECs and urethral epithelial cells as seen in tissue from SEM (Figure 12A) underwent this analysis.
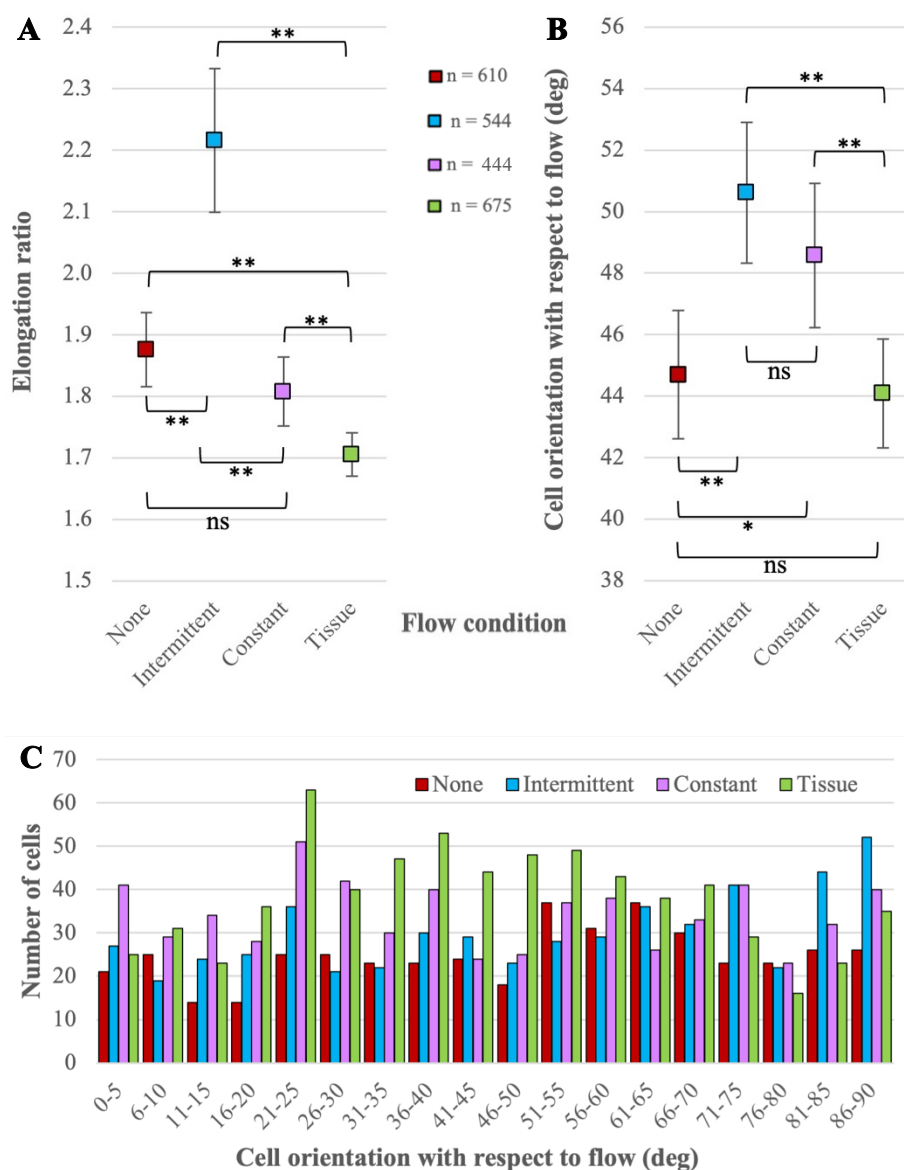
*Figure 11: Cell elongation ratios and orientations with respect to flow were compared between different flow conditions (**A-B**) using paired Welch's t-tests in which α = 0.05. A p-value < 0.05 was considered significant, with 0.01 ≤ p < 0.05 denoted by * and p < 0.01 by **. A histogram depicting the frequency of each orientation across the different conditions is shown in **C**.*

As shown in Figure 11A, there was a statistically significant increase in the degree of elongation shown by cells in the Intermittent Flow condition than those in the Constant and No Flow conditions, which were not statistically distinguishable. This is unsurprising, as long, skinny cells can be plainly seen in the Intermittent Flow ZO-1 image whereas in the Constant and No Flow images they are not noticeable (Figure 8A-C). Elongated cells don't have the only shape seen in the Intermittent Flow condition, however, as a number of the cells are more circular than ovoidal. This makes sense of the fact that the Intermittent Flow condition has a greater standard error than any other condition.

In regard to the high degree of error in the Intermittent Flow group, an exploration was done into the degree of variability between the images used for quantification of cellular elongation within each flow condition using one-way ANOVA tests; the results are shown in Table 1. While the Constant and No Flow conditions were determined to have statistically identical sample groups (considering each image to be a sample group), the Intermittent Flow and Tissue sample groups showed a statistically significant amount of variability between them. It could be speculated that the on-off mechanical stimulation experienced by cells in tissue and under intermittent flow encourages cell morphology to become more variable in contrast to the unchanging conditions of cells under constant flow and static culture.

However, when comparing the cultured cells with those visualized by SEM (Figure 12A), it was found that cells in tissue were significantly less elongated than all groups in-vitro, with the greatest difference seen between Intermittent Flow and Tissue cells. It's therefore difficult to conclude whether exposure to intermittent flow leads in-vitro cells closer to or further away from the in-vivo phenotype.

Table 1: Intra-condition variability data was found via one-way ANOVA between the sample images of each flow condition. α = 0.05 and p-values < 0.05 were considered significant, denoted by *, indicating that the sample groups of the specified condition are not statistically identical.

Flow condition	None			Intermittent*			Constant			Tissue*			
Sample group	1	2	3	1	2	3	1	2	3	1	2	3	4
Mean elongation ratio (n)	1.93 (231)	1.87 (223)	1.80 (156)	1.98 (158)	2.77 (174)	1.94 (212)	1.79 (178)	1.81 (151)	1.83 (115)	1.72 (155)	1.60 (165)	1.68 (189)	1.82 (166)
Variance	0.55	0.70	0.45	0.66	4.25	0.58	0.26	0.31	0.61	0.25	0.16	0.25	0.21
P-value	0.24			$4.92*10^{-10}$			0.88			$4.38*10^{-4}$			

Orientations of cells with respect to flow (Figure 11B) did not exactly follow the trend found for elongation. Although there was a statistically significant difference between Intermittent and No Flow, cells in the latter condition were more aligned to the direction of flow, having an average orientation closer to 0°, than the former. In addition, there was no difference between the Intermittent and Constant Flow conditions for this metric. There was also no difference between No Flow and Tissue cells. It's difficult to draw conclusions from this information alone, but it's important to note that although significant differences were found, the means of each condition fall right around 45°C, which would be the expected average for a group of cells with random orientations. Looking at the frequency of different cell orientations in a histogram (Figure 11C) provides more context. If there were a certain angle of orientation that were preferred by cells, there would be a noticeable peak around this angle. However, what's seen is that the orientation of cells is spread over the graph, suggesting that there is no great deal of orientation occurring in any condition.

In renal epithelium, Frohlich, et al. found that cells require linear topography on their culture surface in order to align, and do not align under flow conditions alone.[42] This is in line with the findings shown in this study.

It may be important to consider the connection between the lower elongations in the Tissue cells and their seemingly random alignment results. In a cell that has no side longer than another, i.e., with an elongation ratio of 1, there is no major or minor axis, and therefore no orientation. However, if a single pixel gives the cell additional length in one direction, this will be measured as the cell's angle of orientation. Because the cells seen under SEM are relatively more round,

human error might play a greater role in the calculated cell orientations, as the tracings can never be 100% accurate or consistent. It could be worth considering a method of normalization for cell orientations if this is used as a metric in future studies.
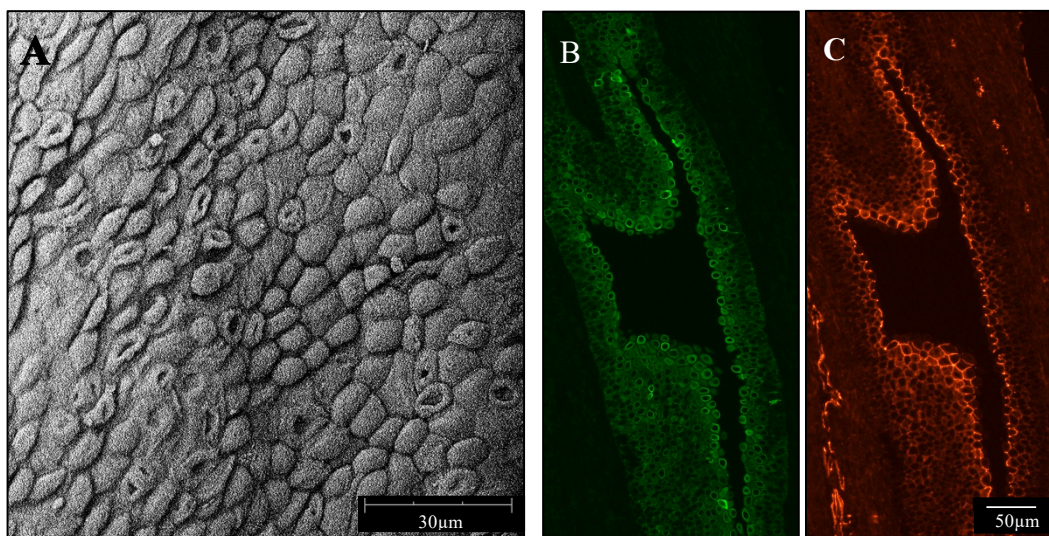

*Figure 12: Images were taken of the urethral epithelium of a piece of porcine penile tissue on a scanning electron microscope (SEM) (**A**), which were then used for quantifying cell orientation with respect to flow and elongation for comparison to cultured cells. A sample from the same tissue source was embedded in paraffin, sectioned, and stained for cytokeratin-7 (CK-7) (**B**), zonula occludins-1 (ZO-1) (**C**), and imaged on a fluorescent microscope.*

These morphological results are somewhat at odds with the findings of prior work in this lab[21], which showed that pUECs elongate and align with the direction of flow significantly more when under constant shear stresses compared to cells under static conditions. The average elongation of cells in this work was 3.9 ± 1.9 for cells under constant flow and 2.2 ± 0.8 for static cells. In this experiment, the elongations were measured at 1.8 ± 0.03 and 1.9 ± 0.03 for constant and static flow conditions, respectively, even at a similar shear stress (10dyn/cm^2 previously versus 9.2dyn/cm^2 in this experiment). The same study described significant differences in alignment between constant and static flow conditions. Cells under flow were more aligned than those under no flow, the opposite of the results presented above. Statically cultured cells were aligned at an angle of $47.5 \pm 24.9°$ on average, similar to the $44.7 \pm 26.3°$ found here, but in cell under constant flow the average alignment was $16.3 \pm 11.3°$ in the referenced study compared to $48.6 \pm 25.2°$ found here.

Later work obtained results similar to those presented in this study, showing no significant difference between the orientation of pUECs under constant flow versus no flow, although the shear stress in this case was estimated to be only 0.049dyn/cm^2.[20] The average shear stress during the Intermittent Flow experiments was 0.76dyn/cm^2 (excluding the acclimation program). This is much closer to 0.049dyn/cm^2 than 10dyn/cm^2, but this condition was still significantly different compared the static condition.

6.2 RT-qPCR

Gene expression analysis can be useful for quantifying changes in a cell that can't be easily seen or measured under a microscope. RT-qPCR amplifies genes that are targeted by specific

primers through thermal cycling and measures the amount of DNA present after each cycle. The intention for RT-qPCR in this study was to determine whether the expression of functional pUEC genes was altered under different flow conditions. Although this stage was not reached by the time of this report, experiments were done to determine whether home-designed primers would efficiently and specifically amplify their target genes and to explore what conditions would allow this to occur.
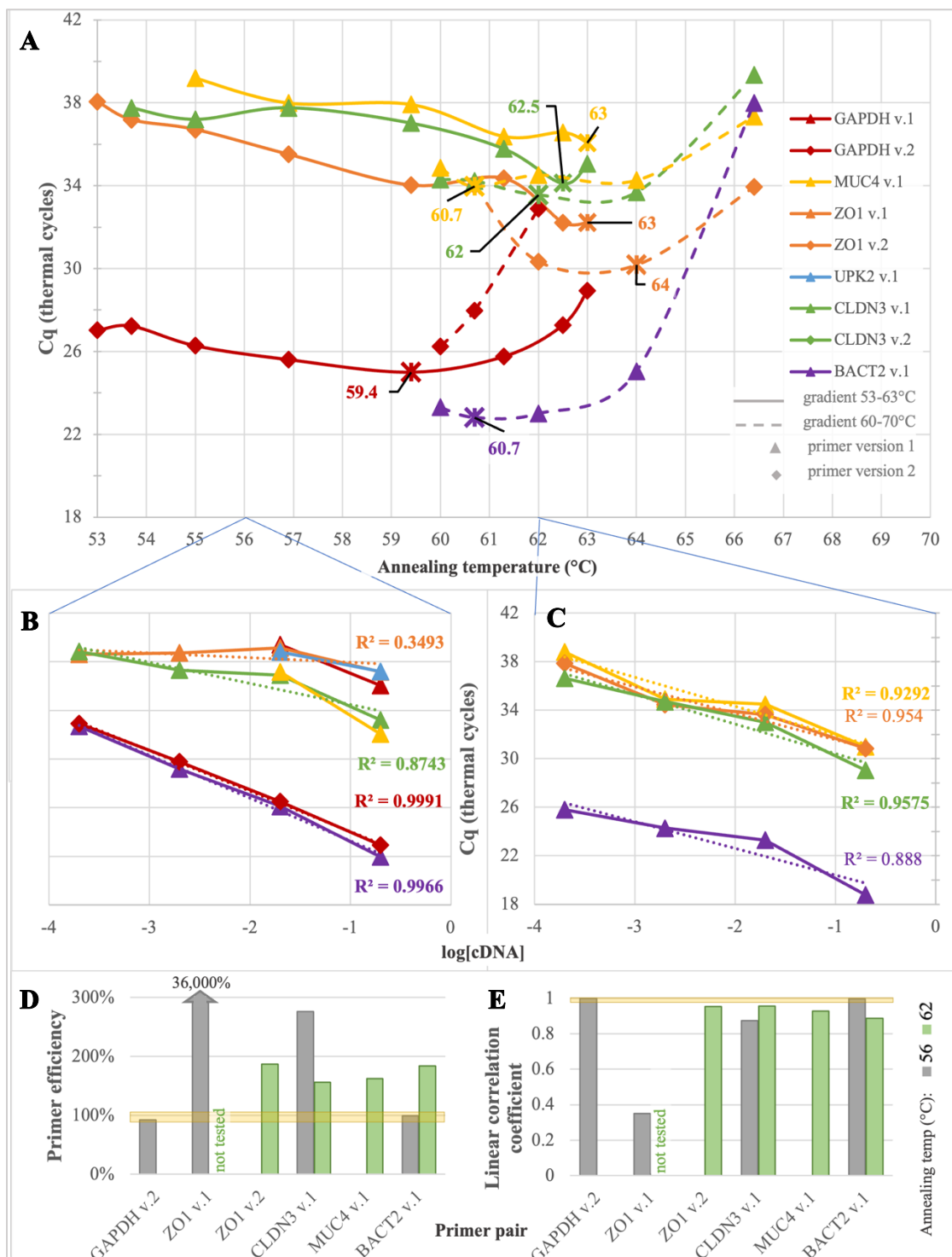
Figure 13: Quantitative polymerase chain reaction (qPCR) assays were performed to assess the efficacies of home-designed S. Scrofa *primers in amplifying pUEC target genes. cDNA titration was originally done at with an annealing temperature of 56°C (**B**) in order to calculate primer efficiencies. Not all primers produced results for each cDNA-positive sample, namely UPK2 v.1, MUC4 v.1, GAPDH v.1, CLDN3 v.2, and ZO1 v.2, which can indicate a non-ideal annealing temperature (T_a). ZO1 v.1, UPK2 v.1, GAPDH v.1, and CLDN3 v.2 were not included in further experiments. Two temperature gradient assays, from 53-63°C and from 60-70°C, were performed to locate ideal annealing temperature for each primer (**A**). In this graph, stars indicate the minimum quantification cycle (Cq) obtained for a given primer and note the corresponding T_a. pUEC cDNA was used at a 1:50 dilution from stock (0.025ng/mL in-well concentration) in both temperature gradient assays. The results from these experiments led to a second cDNA titration (**C**) to determine primer efficiency at a more optimized T_a of 62°C. GAPDH v.2 was also included in this experiment but produced no results. A linear trendline and correlation coefficient is shown in **B** and **C** for each primer that produced three or more data points, and slope of this can be used to calculate primer efficiencies, as depicted in chart **D**. Efficiencies of different primers at each T_a can be compared. Equation 2 was utilized for these calculations. Chart **E** depicts graphically the linear correlation coefficients that are noted on charts **B** and **C**. In this way, linearity at each T_a can be compared. The golden regions on charts **D** and **E** mark the optimal levels at 90-105% efficiency and a linear correlation coefficient > 0.98, respectively.*

RNA was isolated from pUECs cultured in petri dishes under static conditions and was quantified using spectrophotometry to ensure sufficient concentration and purity. This was used to synthesize DNA, which was used as the sample in these qPCR experiments. In a cDNA titration qPCR experiment to test primer efficiency, one would expect an efficient and specific primer in optimal working conditions to have a linear decrease in Cq value with each 10-fold increase in cDNA concentration when plotting logarithmically; in other words, the linear correlation coefficient (R^2) of $\log_{10}$[cDNA] versus Cq would be 1. It's recommended than the R^2 for a primer's standard curve be greater than 0.98.[28] This would correspond to an amplification efficiency between 90 and 105%. Initial standard curve experiments at an annealing temperature of 56°C (Figure 13B) showed low R^2 values for all but two primers, *GAPDH v.2* and *BACT2 v.1*. As expected, these also show the only efficiencies within the recommended range, at 92 and 97%, respectively. The targets of these primers are commonly used housekeeping genes because of their abundance in eukaryotic cells, and as such require less fine tuning of qPCR variable to produce acceptable results compared to gene targets that are less prevalent. These results suggested the need for further testing.

Temperature gradient qPCR experiments can show whether primer performance changes when the temperature of a particular step, in this case annealing, is varied. Two separate annealing temperature gradient assays were performed, one from 53 to 63°C, and one from 60 to 70°C. It should be noted that *BACT2 v.2* was only included in the second assay. For this assay, one would expect to see a well-performing primer exhibit a dip in Cq at its optimal annealing temperature, forming a U shape in a plot of T_a versus Cq. Although the two experiment curves for each primer don't line up perfectly, this general U shape can still be seen, and the dip occurs at approximately the same longitudinal position. The T_a associated with the minimum Cq value on a given curve is considered the optimal T_a for that primer, which are labeled in Figure 13A. The minimum Cq for the eight primers tested was associated with an average T_a value of 61.91°C. This led to the performance of another primer efficiency test at a T_a of 62°C.

The results of this test, shown in Figure 13C, showed overall better primer performance. The notable exception is that *GAPDH v.2*, which performed well in the 56°C primer efficiency test, produced no Cq values despite being included in the 62°C assay. Although this primer's optimal T_a was found to be 59.4°C with a strong upswing in Cq values at higher temperatures, there are still Cq values present up to 63°C. This evidence suggests an error during a pipetting step of PCR plate filling. In the case of every other primer tested in the efficiency curve at 62°C, a Cq value was obtained for every cDNA concentration, an improvement over the 56°C assay. Looking at Figure 13D-E, these parameters are compared side-by-side, although the improvement of *ZO1 v.2* and *MU4 v.1* cannot be visualized here due to the lack of data points on Figure 13B. *CLDN3 v.1*, however, can be seen to have an amplification efficiency and R^2 closer to the golden regions. Despite these improvements, none of the aforementioned primers made it into the recommended regions for either parameter, nor did *BACT2 v.1*, whose performance actually declined. It could be informative to include *BACT2 v.1* on a T_a gradient assay that starts from a lower temperature, as it's minimum Cq appeared at the second-lowest temperature of the gradient this primer was included on, 60.7°C (Figure 13A). Errors in pipetting should also be considered as the cause of this discrepancy. These experiments should be repeated under the same conditions in order to conclude primer function with any certainty.

In-silico PCR was performed on primer pairs as a way of determining their theoretical efficacy. Table 2 shows whether each primer pair produced a target match in the genetic database of *S. scrofa* and how this compared to the peak primer efficiency, or closest value to 100%, obtained by each primer pair.

Table 2: Comparison between peak primer efficiency (the closest value to 100%) and whether a genome match was obtained during in-silico PCR.

Primer	GAPDH v.1	GAPDH v.2	BACT2 v.1	CLDN3 v.1	CLDN3 v.2	MUC4 v.1	UPK2 v.1	ZO1 v.1	ZO1 v.2
isPCR Match?	Yes	No	Yes	Yes	Yes	Yes	Yes	Yes	Yes
Efficiency (%)	N/A	92	97	156	N/A	162	N/A	35,732	187

Interestingly, there does not seem to be a relationship between having a match and having optimal efficiency. Of note is that the only primer to not have a match, GAPDH v.2, has one of the highest efficiencies. This suggests that practical assays should still be used in combination with in-silico primer screening. In addition, looking more closely at the genomic section targeted by the primer and the structure of the primer itself might reveal further clues as to why some primers perform better than others beyond just looking at a yes or no.

6.3   Future perspectives

The quantification performed in this study was based on purely morphological metrics, and while this provides valuable information about how cell shape can change, it says little about how the function of the cells and overall monolayer is affected. Before writing off the efficacy of modulating flow in developing mature pUECs, it would be worth gathering evidence on how the function of these cells is affected under different flow conditions. As mentioned, the process was begun to perform qPCR analysis for quantification of relative gene expression for functional

markers and should be continued. Target genes beyond those investigated here could also be considered, as there are many involved in healthy UEC function, such as Piezos, ion channels thought to be important for mechanical signaling in urothelium.[43] qPCR can measure the prevalence of barrier protein genes, but an experiment involving a FITC-dextran permeability assay can also directly measure the practical function of the pUEC barrier. Techniques such as transepithelial electrical resistance (TEER) can also be applied in this way.[44,45]

Quantitative data was not able to be obtained from buccal mucosa cells for this study. Given their clinical relevance, this is an avenue that should continue to be pursued. In order for this to succeed, a marker should be found that can specifically distinguish cell borders. As mentioned previously, it was found that tight junctions, and therefore ZO-1, are found in more apical BMCs while adherens junctions are located more basally. An antibody that targets an involved protein in this type of barrier, such as a cadherin or catenin, may bring more success in fluorescent immunocytochemistry. Additionally, increased clinical relevance could be achieved by co-culturing BMCs and UECs together to investigate their interactions, since BM grafts must interact with native UE following urethroplasty, both physically and chemically. Previous studies have exposed cultured cells to the secretome of a secondary cell type in the hopes of improving maturity of the cultured cells from exposure to chemicals, proteins, extracellular vesicles, and other components of the secondary cells.[46,47] Something similar could be done when culturing BMCs vis a vis the sectretome of UECs to mimic some of the chemical aspects of the native urethral environment. In further comparing BMCs and UECs is will also be preferable to use cells of the same species. Since obtaining UECs from humans has proven difficult, the most convenient route to this might be obtaining BMCs from a porcine source. The difficulty in this is that primary porcine cells can be prone to infection, decreasing the chances of establishing a health line of cells.

There are other regenerative methods that could be employed to solve the problem of cell unavailability. Many cell types, including epithelial cells, have now been derived from the directed differentiation of induced pluripotent stem cells.[48-50] There a multitude of different variables that can be added and tuned in an iPSC differentiation protocol in order to obtain the cell type desired, which in turn entails the usage of a great deal of time and resources towards optimization and characterization. Stem cell derived UECs would also open the door for culturing of urethral organoids, which can be abundant cell sources in themselves.

When looking back to the in-vivo conditions, UECs experience more than just flow in their natural state. In fact, they exist in zero fluid shear conditions for the majority of the time, though they do experience other mechanical stimuli, as mentioned previously. Mechanical stimuli also include cell-substrate interactions, so moving away from flat, hard plastic towards a culture substrate more similar to that in-vivo, with regard to stiffness and geometry, would be worth exploring. A flexible culture surface would also lend itself to other in-vitro mechanical stimulation techniques, such as stretching and compression. Culturing cells in a 3D environment such as a biomaterial scaffold or hydrogel has been shown to improve their maturity as well, though the specific characteristics of each would require optimization and tuning.[51] Systems with increased complexity often require more money, time, and advanced machinery than simpler devices, however it could result in bringing a true urethra on a chip to life.

7 Conclusions

The aim of this research was to determine whether intermittent fluid shear stresses, like those experienced in the urethra, have a different effect on the phenotype of porcine urethral

epithelial cells when compared to constant fluid shear stresses. In comparing the elongation ratio of cells from No Flow, Constant Flow, Intermittent, and Tissue conditions, it was confirmed that flow induced more elongated cells. Cells under intermittent flow were more elongated than those under constant flow, but also those in tissue. Orientation of cells' major axes to the direction of flow was also compared, showing that there was no difference between Intermittent and Constant Flow groups for this morphological parameter, but the difference between Intermittent and Tissue cells remained. However, due to the averaging of orientations for all conditions to values near 45°, it is thought that flow has no significant effect on orientation. Therefore, it seems that intermittent flow alone does not drive pUECs towards a tissue-like morphology. Other parameters besides flow profile will likely need to be considered when designing a urethral organ-on-a-chip.

Described in this report is a significant step towards the first urethra-on-a-chip to be developed. Recapitulation of urinary flow patterns on urethral cells has never been described in literature, and the results add to the body of knowledge that will lead to the development of regenerative urologic therapies.

8 References

1 Zimmerman, W. B. & Santucci, R. A. Buccal mucosa urethroplasty for adult urethral strictures. *Indian journal of urology: IJU: journal of the Urological Society of India* **27**, 364 (2011).

2 Hermosa, P. C., Campos-Juanatey, F., Malo, R. V., Gómez, M. Á. C. & Baños, J. L. G. Sexual function after anterior urethroplasty: a systematic review. *Translational Andrology and Urology* **10**, 2554 (2021).

3 Alwaal, A., Blaschko, S. D., McAninch, J. W. & Breyer, B. N. Epidemiology of urethral strictures. *Translational andrology and urology* **3**, 209 (2014).

4 Bultitude, M. F. (Blackwell Publishing Ltd Oxford, UK, 2012).

5 Gray, H. (Lea & Febiger, Philadelphia, 1918).

6 Samarska, I. V., Dani, H., Bivalacqua, T. J., Burnett, A. L. & Matoso, A. Histopathologic and clinical comparison of recurrent and non-recurrent urethral stricture disease treated by reconstructive surgery. *Translational Andrology and Urology* **10**, 3714 (2021).

7 Lumen, N. *et al.* Etiology of urethral stricture disease in the 21st century. *The Journal of urology* **182**, 983-987 (2009).

8 Pierik, F. H. *et al.* A high hypospadias rate in The Netherlands. *Human reproduction* **17**, 1112-1115 (2002).

9 Kogan, M. *et al.* The influence of urethral stricture disease and urethroplasty on anxiety and depression in men. *Urologiia (Moscow, Russia: 1999)*, 60-63 (2018).

10 Weese, J. R. *et al.* Anterior urethral stricture disease negatively impacts the quality of life of family members. *Advances in Urology* **2016** (2016).

11 Henderson, N. C., Rieder, F. & Wynn, T. A. Fibrosis: from mechanisms to medicines. *Nature* **587**, 555-566 (2020).

12 Jacobs, M. E., de Kemp, V. F., Albersen, M., de Kort, L. M. & de Graaf, P. The use of local therapy in preventing urethral strictures: a systematic review. *PloS one* **16**, e0258256 (2021).

13 Xie, M. *et al.* Evaluation of stretched electrospun silk fibroin matrices seeded with urothelial cells for urethra reconstruction. *journal of surgical research* **184**, 774-781 (2013).

14   Raya-Rivera, A. *et al.* Tissue-engineered autologous urethras for patients who need reconstruction: an observational study. *The lancet* **377**, 1175-1182 (2011).

15   Chen, F., Yoo, J. J. & Atala, A. Acellular collagen matrix as a possible "off the shelf" biomaterial for urethral repair. *Urology* **54**, 407-410 (1999).

16   Osman, N. I., Patterson, J. M., MacNeil, S. & Chapple, C. R. Long-term follow-up after tissue-engineered buccal mucosa urethroplasty. *European urology* **66**, 790-791 (2014).

17   Zhang, Y., Yoo, J. J. & Atala, A. Tissue engineering: bladder and urethra. *Principles of Tissue Engineering*, 845-862 (2020).

18   Stone, A. R. Editorial comment on: tissue-engineered buccal mucosa urethroplasty-clinical outcomes. *European urology* **53**, 1270-1270 (2008).

19   Leung, C. M. *et al.* A guide to the organ-on-a-chip. *Nature Reviews Methods Primers* **2**, 1-29 (2022).

20   Casademont Roca, A. Towards a urethra-on-a-chip to study development, prevention, and treatment of fibrosis in urethral stricture disease. (Utrecht University & University Medical Center Utrecht, 2021).

21   Fisher, A. G. Tissue Engineering for Urethral Reconstruction : Hydrogel Optimization and Perfusion Flow on Epithelial Cells. (Utrecht University & University Medical Center Utrecht, 2020).

22   Kumar, V., Dhabalia, J. V., Nelivigi, G. G., Punia, M. S. & Suryavanshi, M. Age, gender, and voided volume dependency of peak urinary flow rate and uroflowmetry nomogram in the Indian population. *Indian Journal of Urology* **25**, 461 (2009).

23   Talati, J. Urethral dilatation. *JPMA. The Journal of the Pakistan Medical Association* **39**, 79-83 (1989).

24   in *Encyclopedic Dictionary of Polymers*   (ed Jan W. Gooch) 477-477 (Springer New York, 2007).

25   Chammas Jr, M. F. & Kim, F. J. Urodynamics and Voiding Dysfunction. *Abernathy's Surgical Secrets E-Book*, 469 (2008).

26   Chun, K., Kim, S. J. & Cho, S. T. Noninvasive medical tools for evaluating voiding pattern in real life. *International Neurourology Journal* **21**, S10 (2017).

27   Haylen, B. T. *et al.* An International Urogynecological Association (IUGA)/International Continence Society (ICS) joint report on the terminology for female pelvic floor dysfunction. *Neurourology and Urodynamics: Official Journal of the International Continence Society* **29**, 4-20 (2010).

28   Kuang, J., Yan, X., Genders, A. J., Granata, C. & Bishop, D. J. An overview of technical considerations when using quantitative real-time PCR analysis of gene expression in human exercise research. *PloS one* **13**, e0196438 (2018).

29   Shen, L., Weber, C. R., Raleigh, D. R., Yu, D. & Turner, J. R. Tight Junction Pore and Leak Pathways: A Dynamic Duo. *Annual Review of Physiology* **73**, 283-309 (2011). https://doi.org:10.1146/annurev-physiol-012110-142150

30   Smith, N. J. *et al.* The human urothelial tight junction: claudin 3 and the ZO-1α+ switch. *Bladder* **2**, e9 (2015).

31   Russo, C. L. *et al.* Mucin gene expression in human male urogenital tract epithelia. *Human reproduction* **21**, 2783-2793 (2006).

32   Li, W. *et al.* Uroplakin II is a more sensitive immunohistochemical marker than uroplakin III in urothelial carcinoma and its variants. *American journal of clinical pathology* **142**, 864-871 (2014).

33   Birder, L. & Andersson, K.-E. Urothelial signaling. *Physiological reviews* **93**, 653-680 (2013).

34   Barber, R. D., Harmer, D. W., Coleman, R. A. & Clark, B. J. GAPDH as a housekeeping gene: analysis of GAPDH mRNA expression in a panel of 72 human tissues. *Physiological genomics* **21**, 389-395 (2005).

35   Cunningham, F. *et al.* Ensembl 2022. *Nucleic acids research* **50**, D988-D995 (2022).

36   Ye, J. *et al.* Primer-BLAST: a tool to design target-specific primers for polymerase chain reaction. *BMC bioinformatics* **13**, 1-11 (2012).

37   Yu, B. & Zhang, C. in *In Silico Tools for Gene Discovery*   91-107 (Springer, 2011).

38   Schindelin, J. *et al.* Fiji: an open-source platform for biological-image analysis. *Nature methods* **9**, 676-682 (2012).

39   Stoddard, N. & Leslie, S. W. Histology, male urethra. (2019).

40   Imafuku, K. *et al.* Zonula occludens-1 demonstrates a unique appearance in buccal mucosa over several layers. *Cell and Tissue Research* **384**, 691-702 (2021).

41   Jones, K. B. & Klein, O. D. Oral epithelial stem cells in tissue maintenance and disease: the first steps in a long journey. *International journal of oral science* **5**, 121-129 (2013).

42   Frohlich, E. M., Zhang, X. & Charest, J. L. The use of controlled surface topography and flow-induced shear stress to influence renal epithelial cell function. *Integrative Biology* **4**, 75-83 (2012).

43   Li, X., Hu, J., Zhao, X., Li, J. & Chen, Y. Piezo channels in the urinary system. *Experimental & Molecular Medicine* **54**, 697-710 (2022).

44   Li, B.-R. *et al.* In vitro and in vivo approaches to determine intestinal epithelial cell permeability. *JoVE (Journal of Visualized Experiments)*, e57032 (2018).

45   Srinivasan, B. *et al.* TEER measurement techniques for in vitro barrier model systems. *SLAS Technology* **20**, 107-126 (2015).

46   Pawitan, J. A. Prospect of stem cell conditioned medium in regenerative medicine. *BioMed research international* **2014** (2014).

47   Cases-Perera, O. *et al.* Development of secretome-based strategies to improve cell culture protocols in tissue engineering. *Scientific reports* **12**, 1-14 (2022).

48   Kondo, Y., Toyoda, T., Inagaki, N. & Osafune, K. iPSC technology‐based regenerative therapy for diabetes. *Journal of diabetes investigation* **9**, 234-243 (2018).

49   Firth, A. L. *et al.* Functional gene correction for cystic fibrosis in lung epithelial cells generated from patient iPSCs. *Cell reports* **12**, 1385-1390 (2015).

50   Li, Y., Chan, L., Nguyen, H. V. & Tsang, S. H. Personalized medicine: cell and gene therapy based on patient-specific iPSC-derived retinal pigment epithelium cells. *Retinal Degenerative Diseases*, 549-555 (2016).

51   Haycock, J. W. 3D cell culture: a review of current approaches and techniques. *3D cell culture*, 1-15 (2011).

9 Appendix

Supplementary Table 1: Primer pairs that were used in RT-qPCR.

Code	Primer	Forward	Reverse	In-silico PCR match?
P1 F/R	GAPDH v.1	CGACCTTCACCATCGTGTCT	CTTTGCCCCGGCGATCTAATG	Yes
PdG 5/6	GAPDH v.2	ACACTCACTCTTCTACCTTTG	CAAATTCATTGTCGTACCAG	No
PdG 3/4	BACT2 v.1	ATCCACGAGACCACCTTCAA	TGATCTCCTTCTGCATCCTG	Yes
P7 F/R	CLDN3 v.1	ACTTCTTTTCTCTCGGCGGG	CAACACCATCATCCGGGACT	Yes
P12 F/R	CLDN3 v.2	GCCTTCATCGGCAGCAGCATTA	AGTGCAAAGTGTACGACTCTCT	Yes
P8 F/R	MUC4 v.1	GCTCCACTGCCCTATTCACA	AAGTGGGCAAGTGCAAGAGA	Yes
P9 F/R	UPK2 v.1	GTCCACGCTTCCTCGTAAGT	ATCGGACACAATCGCTACCC	Yes
P6 F/R	ZO1 v.1	ATGGGCGTTACCCTGCAAGAA	AGCTCCACTGTGATTCTTCGT	Yes
P23 F/R	ZO1 v.2	GTCCAGAATCTCGGAAAAGTGCC	CTTTCAATGCTCCATACCAACC	Yes
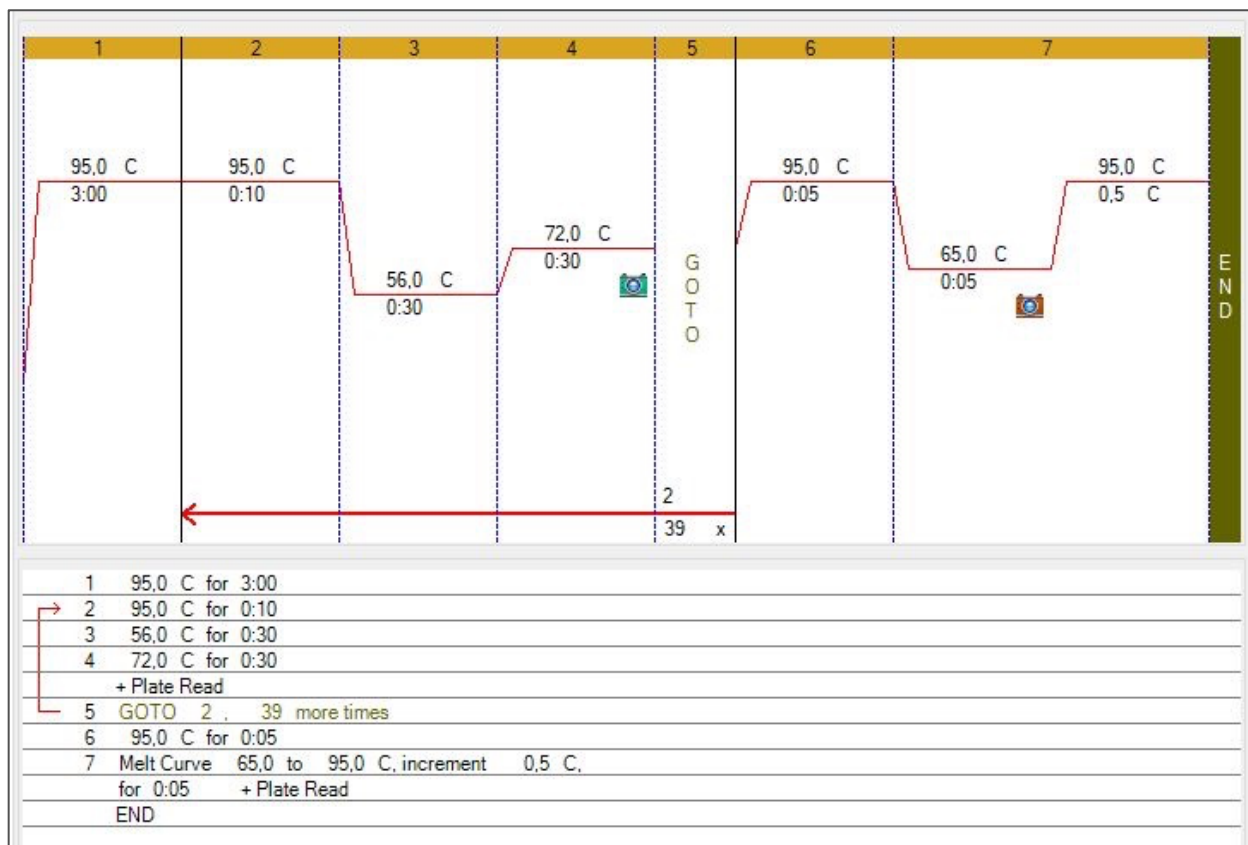
Supplementary Figure 1: An example of a CFX Maestro (Bio-Rad) qPCR protocol for measuring primer efficiency via a cDNA standard curve. Over multiple tests, exact temperatures differed slightly.
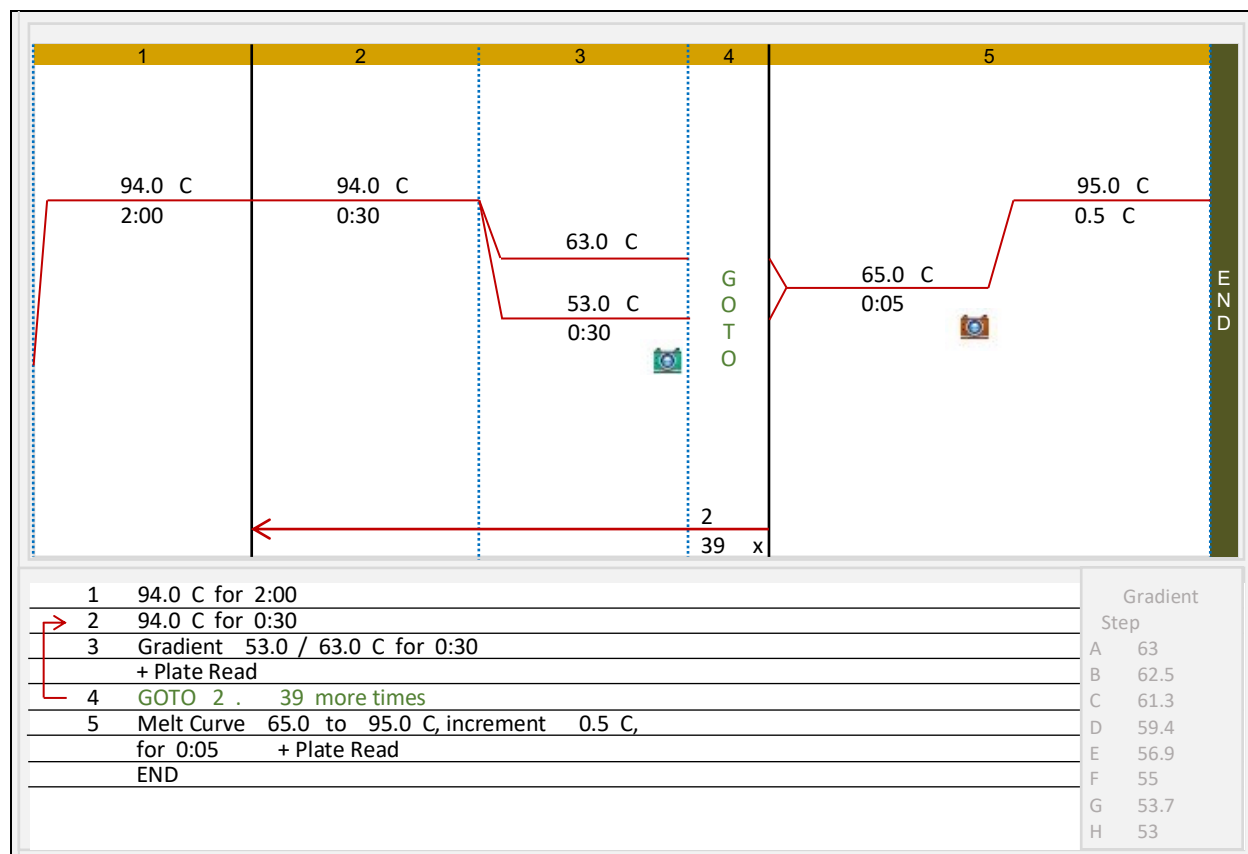
Supplementary Figure 2: An example of a CFX Maestro qPCR protocol for an annealing temperature optimization test. Over multiple tests, exact temperatures differed slightly.